Ｍ６タンパク質はマウスの脳梁投射細胞において軸索伸長を制御する

総合研究大学院大学生命科学研究科

遺伝学専攻

三田さくら

(学籍番号) 20071854

平成２３年度

M6 proteins regulate axon outgrowth in mouse callosal neurons

Sakura MITA

Doctor of Philosophy

Division of Brain Function, National institute of Genetics

Department of Genetics, School of Life Science

The Graduate University for Advanced Studies (SOKENDAI)

2011 (School Year)

Table of contents

Abstract

Corpus callosum (CC) is the largest fiber tract in the human brain that connects the left and right cerebral hemispheres. The absence of the CC results in impairment of higher-order cognitive functions because interhemispheric transfer of information is disrupted. The formation of the CC is intricately regulated by a large number of molecules, which have not been fully characterized, while actively searched. In this study, I showed that additional molecules, M6 proteins, are also involved in the CC development.

M6 proteins consist of M6a and M6b, highly homologous four-transmembrane proteins. M6a was originally found by the antibody screening for candidate molecules that are involved in guidance of axons. Previously, we found that when anti-M6a antibody binds to M6a protein in cultured neurons, the axons stall the elongation. Therefore, it seemed that M6a is involved in axon elongation of developing neurons. However, no study has so far examined the function of M6 proteins in vivo. To address this issue, I analyzed brain morphology and axonal projections in knockout mice for the M6a and M6b genes.

First, to assess whether the two M6 proteins have redundant functions, I investigated expression patterns of M6a and M6b proteins in the wildtype mouse brains during developmental stages, using a newly prepared anti-M6b specific antibody. M6a was expressed mainly in growing axons as previously reported. The new anti-M6b antibody revealed that M6b

was well co-localized with M6a in these axons. The expression level of M6b on the axons appeared lower at E14.5 compared with M6a, and subsequently intensified at E16.5 and P0, displaying comparable overlapping patterns with M6a. I also examined the subcellular distribution of M6 proteins in neurons in dissociated culture. As described previously, M6a protein was enriched in the edge of growth cones and the shaft filopodia of axons in cultured neurons. M6b protein was also expressed in the growth cones and the shaft filopodia, and co-localized with M6a. Previous studies have shown that binding of anti-M6a antibodies to M6a induces aggregation of the protein over the growth cone membrane. I found that, during this reaction, M6b proteins also changed the distribution and were aggregated together with M6a proteins. Because the anti-M6a antibody does not bind to M6b protein, the redistribution of M6b proteins can not be due to the direct action of the anti-M6a antibody binding. Instead, when M6a proteins change the location upon binding of the anti-M6a antibody, they might be accompanied by physically interacting M6b proteins. These observation suggest that M6a and M6b are co-localized and behave together in the subcellular level, supporting the idea that these proteins function redundantly.

Because redundant functions for M6a and M6b were postulated, I examined the brain phenotypes in the *M6a*-/- *M6b*-/- double knockout mice. Histological analyses of the brain sections revealed that the major axon tracts basically existed in the double knockout mice. However, the size of the CC bundle was abnormally small in the *M6a*-/- *M6b*-/- knockout mice.

This hypoplasia in the CC was not clear at early developmental stages (E14.5, E16.5 and P0), but became obvious by P7 and throughout life. I quantified the size of the CC in wild-type, single and double mutant mice at P7, and found that the defect was most pronounced in the double knockout mice, indicating the redundant function of the two M6 proteins.

I considered the following three possibilities to explain the smaller CC bundles in the double knockout mice. 1) the number of the callosal neurons is reduced. 2) The axons of the callosal neurons are misdirected from callosal pathway. 3) The axon outgrowth is impaired in the callosal neurons.

First, to evaluate the possibility 1), I measured the density of cortical neurons in the mutant cortex in the motor, somatosensory, and visual areas. The neural density of the double mutant cortex was comparable to that of the wild-type. This result suggests that the number of callosal neurons was not reduced in the *M6a*-/- *M6b*-/- mice.

Second, to evaluate the possibility 2), I labeled the callosal projection in the cortex of *M6a*-/- *M6b*-/- double knockout mice by selectively electroporating GFP-expressing vector into cortical neurons and visualized the trajectory of CC. After I compared the pathway of the mutant and wildtype, I found that significantly smaller number of axons reached the contralateral cortex in the double mutant. Also, there were ectopic bundles of axons coursing ventrally toward the striatum region in the double mutant. However, this method labeled too many neurons so I could not discriminate and trace one neuron from the cell body to the axon.

There was possibility that I labeled the neurons located lateral side of the callosal neurons and normally project into the striatum as well. So, to exclude this possibility, next I used single cell labeling system, which labeled callosal neurons sparsely enough to trace one neuron from cell body to the destination. And I confirmed that these ectopic projections of double mutant to the septum indeed originated from the cell bodies in the position specified for the callosal neurons. The results suggest that at least some callosal axons were misdirected from callosal pathway in the double knockout mice. Therefore, the possibility "2) The axons of the callosal neurons are misdirected from callosal pathway" was indeed the one cause of the defect of CC.

Lastly, to evaluate the possibility 3), I examined the axon outgrowth in the callosal neurons. Cortical neurons were isolated from the mutants and cultured to evaluate the intrinsic capability of the neurite length. The quantification indicated that the axonal length of any single and double mutant neurons was significantly smaller than that of the wild-type neurons. The impairment in the neurite outgrowth was similarly observed in cortical neurons, regardless of the layer position or the birth time, suggesting that the defect of *M6a*-/- *M6b*-/- was not limited in the callosal neurons, but rather common to all cortical neurons. I next examined whether the expression of M6 proteins rescued the impairment of axonal growth in *M6a*-/- *M6b*-/- neurons. When plasmids expressing M6a or M6b were transfected into the cortical neurons of the double knockout mice, either of the proteins succeeded to make callosal neuron

restore the axonal length to the normal level. These results confirm that M6a or M6b proteins have redundant functions in the axon outgrowth.

Finally, using culture system, I mapped the functional domain of M6a that was required for the axonal growth. I picked up several kinds of the expression plasmids for M6a which deleted in the deferent domains of M6a and transfected into cortical neurons of *M6a*-/- *M6b*-/-. Through assays of various deletion constructs, I found that the second intracellular loop (amino acid 105-128) was required to restore the axonal outgrowth in the double knockout neurons.

In this study, I showed that M6 proteins have an essential role in the formation of the CC by regulating the axonal growth of callosal neurons. M6a and M6b are functionally redundant in this process. Based on the results from the primary cultured neurons, the defect of the CC in the *M6a*-/- *M6b*-/- double knockout mice is at least partly due to the reduced length of axons, which can be attributed to the impairment in the intrinsic ability of individual callosal neurons to extend the sufficient length of axons. Furthermore, the study revealed that some callosal axons are misguided ventrally in the double knockout mice, which should also contribute to the hypoplasia in the CC.

Introduction

The development of the mammalian central nervous system involves precise wiring of neurons. For the proper targeting of axons, growth cones recognize various molecules in their environment and use these molecules as the guidance cues to navigate toward their particular destinations.

The corpus callosum (CC) is a assembly of the callosal axons which provide the long neural pathways to connect the left and right cerebral hemispheres in mammals. The projection of the callosal neuron starts from the cortical plate down toward the white matter, then makes a sharp turn to the midline. Crossing midline, the axon again turns to innervate into the cortical plate of the other side. The positions of the cell body of the callosal neuron and its target in the other hemisphere are arranged in a symmetric manner. The association of two hemispheres is thought to be essential for dealing with complex intellectual tasks. In humans, the importance of CC has been studied in the patients who have a congenital defect or surgical lesion in the CC. The absence of CC results in the impairment of the higher-order cognitive functions because interhemispheric transfer of information is disrupted (Paul et al., 2007). It is shown that the formation of the CC requires a complex combination of the guidance molecules (Donahoo et al., 2009), as well as the organized cytoskeletal molecules in the growth cones of cortical callosal neurons (Lanier et al., 1999; Takei et al., 2000; Teng et al., 2001).

M6a is a four-transmembrane protein that belongs to the myelin proteolipid protein (PLP) family. PLP is the most abundant protein in the myelin sheath of the central nervous system (CNS). Although PLP and its splicing isoform DM20 are expressed in oligodendrocytes, M6a is exclusively expressed in CNS neurons (Yan et al., 1993). The M6a gene encodes 278 amino acid protein with both the N- and C-termini facing the cytosol. Molecular cloning of M6a led to the identification of a highly homologous protein, M6b (Yan et al., 1993). M6b is expressed in both neurons and glial cells (Yan et al., 1996). The amino acid sequences of M6a and M6b are 56% identical to each other, and 43% (M6a) and 51% (M6b) identical to DM20, respectively.

Despite the fact that M6a was identified years ago (Lagenaur et al., 1992), little is known about its biological function. A previous study reported that over-expression of M6a in rat pheochromocytoma PC12 cells increases their responsiveness to nerve growth factor (Mukobata et al., 2002). Functions in filopodium/spine formation have also been suggested for M6a (Brocco 2010, Alfonso 2005, Michibata 2009). However, the function of this protein in vivo has been unstudied so far.

Because M6a is highly expressed on the surface of the axons, dendrites and the neuronal growth cones, its potential functions in neurite elongation and guidance have been postulated (Lagenaur et al., 1992). Furthermore, in the previous study, we found notable axon behavior involving M6a; when anti-M6a antibody binds to M6a protein in culture, the axons

stalls the elongation (Sato et al., 2011a). Interestingly, during this reaction, the axons maintain the actin- rich growth cones exhibiting highly motile movement. Generally, inhibition of axon elongation accompanies disruption of the actin cytoskeleton in growth cones, which is called the growth cone collapse. Therefore, it seems that the reaction mediated by M6a is unique and involves a novel mechanism for axon elongation. In this study, I analyzed axon elongation in the brain of knockout mice for the M6 proteins to know their biological functions in vivo.

Experimental procedures

Animals

For analysis of expression of M6 proteins, ICR wild-type mice were purchased from Japan SLC, Inc. M6a knockout mice in the C57BL/6 background were produced previously (Sato et al., 2011a), and maintained in the animal facility at the National Institute of Genetics. Drs. Werner and Nave gifted M6b and PLP knockout mice in the C57BL/6 background. To obtain M6a and M6b double knockout mice, *M6a*+/- *M6b*+/- or *M6a*-/- *M6b*-/- female mice were mated with *M6a*+/- *M6b*-/*Y* or *M6a*-/- *M6b*-/*Y* male mice. To obtain *M6a*-/- *M6b*-/*Y PLP*-/*Y* triple knockout mice, *M6a*-/- *M6b*+/- *PLP*+/- female mice were mated with *M6a*-/- *M6b*+/*Y PLP*+/*Y* male mice. Because both *M6b* and *PLP* are located on the X chromosome, the triple knockout mice were obtained only when both gene were arranged on the same X chromosome in the ovum of the dam by the random crossing over of X chromosome. The day on which a vaginal plug was detected was designated as embryonic day 0.5 (E0.5). The day of birth was designated as postnatal day 0 (P0). All experimental protocols were approved by the Animal Committee of the National Institute of Genetics and were carried out according to their guidelines to minimize pain or discomfort in the animals.

Genotyping PCR

Genotyping was performed by PCR amplification of the genomic DNA prepared from the tails with the specific primers. To obtain the amplification products of specific gene fragments by PCR, I used the primer sets M6G-F6 (5'-ggg att ctg gca gct gga gag-3') and M6G-wt2 (5'-ggt tgg gtg tta att tag gag ag-3') for M6a wild type, and M6G-F6 and M6G-R8 (5'-aaa acc agg aaa aaa aca tgc ttt c-3') for M6a knockouts, P62 (5'-ccc ttt gcc tcc cag tca gtt g-3') and P38 (5'-cca ggg agg cat agg gaa ct-3') for M6b wild type, P62 and neo6 (5'-gca atc cat ctt gtt caa tgg c-3') for M6b knockouts, Pro215 (5'-gga gag gag gag gga aac gag-3') and Pro370 (5'-tct gtt ttg cgg ctg act ttg-3') for PLP wild type, hwneo (5'-ttg gcg gcg aat ggg ctg ac-3') and Pro370 for PLP knockouts. For sex identification, the primers for *sry* gene on the Y chromosome, ZfY-FW (5'-gat aag ctt aca taa tca cat gga-3') and ZfY-RV (5'-cct atg aaa tcc ttt gct gc-3') were used.

Tissue preparations and sectioning

Brains of E14.5 and E16.5 embryos, and P0, P7, P14 and P60 mice were used. For the postnatal and adult mice, animals were anesthetized and transcardially perfused with 4% paraformaldehyde (PFA)/ phosphate buffered saline (PBS). Brains were dissected out and further fixed with 4% PFA overnight. To make paraffin sections (hemaotoxyline and eosin staining, fluoromyelin staining, immunohistochemistry for anti-GFP and NeuN), the tissues were embedded in paraffin and cut into 5μm-thick sections using a microtome(RM2255, Leica

Microsystems). To make frozen sections (immunohistochemistry for anti-M6a, M6b and neurofilament), the tissues were immersed in 30% sucrose followed by the fixation, and frozen in OCT compound (TissueTek; Sakura Finetechnical, Tokyo Japan), and cut into 20 μm-thick sections using a cryostat. For the axonal labeling and the single cell labeling experiments, the brains were cut into 100 μm-thick sections using a vibratome (Dosaka EM).

Immunostaining

The brain sections and cultured neurons were incubated with primary antibodies in 10 mM Tris-Hcl, pH7.4, 130 mM NaCl, 0.1% Tween20 (TBST) at 4°C overnight, followed by secondary antibodies at room temperature for two hours. The primary antibodies used for histological staining are as follows: rat anti-M6a (1:300,MBL); rat anti-M6a monoclonal M6 (1μg/ ml, Developmental Studies Hybridoma Bank); rabbit anti-M6b (1:500, 0.079 μg/ ml), mouse anti-neurofilament 2H3 (1:100, hybridoma supernatant, Developmental Studies Hybridoma Bank); mouse anti-neuron-specific tubulin TUJ-1 (1:1000, COVANCE); rabbit anti-GFP (1:500, MBL); mouse anti-NeuN (1:500, CHEMICON); mouse anti-MAP2 (1:500, Sigma); mouse anti-BrdU (1:100, BD Bioscience). As the secondary antibodies, goat Cy3-conjugated anti-rabbit IgG, Alexa488-conjugated anti-mouse IgG, and Alexa488-conjugated anti-rat IgG antibodies (1:500, Jackson ImmunoRsearch LABORATORIES, Inc.) were used. In some studies, the brain sections were stained with hemaotoxyline and eosin (HE) or with fluoromyelin (1:300, Molecular

probes).

Size measurement of the CC and the anterior commissure (AC)

A series of the sagittal sections were obtained from the mouse brain at P7. Five sections at the midline from each sample were selected. The sections were stained with hemaotoxyline and eosin (HE) and digitally photographed with a CCD camera (DP71, Olympus). The area of the CC and AC were measured on the images using image J software (National Institutes of Health).

Quantification of the cortical neuron density

The coronal paraffin sections of the brain were stained for the neuronal marker NeuN. The number of NeuN-positive cells in a 20 × 500-μm square of each layer of three different cortical areas were counted. The motor, somatosensory, and visual cortical areas and the layers were determined by reference to the mouse atlas (Atlas of the developing mouse brain at E17.5, P0, P6).

BrdU labeling

For birthdate labeling, BrdU (4 mg) was injected to a pregnant mother at E15.5 so that cortical layer II/III neurons were selectively labeled. The brains were dissected and used for culturing cortical neurons or sectioning. Cells with BrdU incorporated nuclei were detected by anti-BrdU

antibody after DNA denaturing by 2 N HCl for 2 h at room temperature.

Dissociated culture of cortical neurons

The neocortical tissues were dissected from the mouse embryos at E18.5, treated with 0.1% trypsin, and dissociated into single cells by gentle pipetting. The cells were plated at a density of 6×10^3 cells/cm^2 on the laminin-coated 8-well chamber slides (Nalge Nunc) and cultured in Neurobasal medium (Life Technologies) supplemented with B27 and N2 supplements (Life Technologies) for 72 h at 37°C in a 5% CO_2 atmosphere. Primary olfactory bulb neurons were cultured as described previously (Sato et al., 2011a).

Callosal axon labeling in utero

In utero electroporation was performed as described previously (Mizuno 2007). In brief, pregnant mice at E15.5 of gestation were anesthetized and the uterus was surgically exposed. A small amount (-0.6 μl) of 1.5 mg/ml DNA solution coding for GFP was injected to the either right or left lateral ventricle of the embryos. Subsequently, electric pulses (35mV; 50ms; 4 times for culture, or 30mV; 50ms; 4 times for axon labeling) were delivered using electroporator (CUY-650, Nepagene). Then the uterus was replaced into the mother. After birth, the pups were collected at P7 and the brains were dissected for experiments. For the axonal labeling, the plasmid of membrane-expressing EGFP (pCAGGS-mem-EGFP) was used.

Single neuron tracing

For the single neuron tracing, supernova method was performed (Mizuno et al. 2014). Briefly, the plasmid sets (TRE-nlsCre [10 ng/μL], CAG-loxP-stop-loxP-TurboRFPires-tTA-WPRE [1 μg/μL]) were electroporated in utero with the electric pulses (30mV; 50ms; twice). the brains were collected at P7, and sectioned. 12-15 z-plane images were taken from each 100-μm-thick section by confocal microscopy (FV 1000 Olympus). After the images were stacked, the axons and the dendrites of each labeled cortical neuron were traced using Neuron J software and reconstructed with Adobe Illustrator software.

Transfection of cultured cortical neurons

The full-length cDNAs for mouse M6a, M6b and DM20 were subcloned in pCAGGS-ires-EGFP vector to coexpress these proteins with GFP. The truncated forms of M6a (Δ105-114, Δ115-128, Δ105-128, Δ238-247) were also subcloned in the same vector. The expression plasmids were electroporated into mouse cortical neurons at E15.5 by in utero electroporation as described above. The cortical neurons of E18.5 mouse embryos were then dissociated and cultured for 72 hours as described.

Quantification of neurite length

The cortical neurons were cultured for 72 h and fixed with 4%PFA/PBS for 1h at room temperature then co-labeled with anti-Tuj-1, anti-GFP and anti-BrdU antibodies. Transfected neurons were detected as GFP positive cells, and layer 2/3 neurons were detected as BrdU positive cells. The fluorescent images were acquired by CCD camera. The neurite were traced and the length was measured with Neuron J, which is plug-in software of image J.

Results

Overlapping expression of M6a and M6b in the central nervous system

M6a and M6b are homologous throughout the entire structures, both have four -transmembrane structure. Also these two proteins are 55% identical in the amino acid sequences. Because of this high similarity, I hypothesized that these two proteins might have redundant functions in vivo. If so, it is possible that M6a and M6b have similar expression pattern in vivo especially in the axon bundles where M6a function was revealed in vitro. Therefore, I investigated the expression patterns of the M6a and M6b proteins at three deferent stages of the developing mouse brains, which is E14.5, E16.5 and P0.

Using wild type mouse brain, I investigated the expression pattern of M6a and M6b. We already had anti-M6a antibody (Sato et al., 2011a), but I need to prepare the antibody for M6b. The anti-M6b antibody was designed against the intracellular C-terminus (CMQ AYQ DIK AKE EQE LQD IQS RSK EQL NSY T) of M6b protein (Werner et al. 2001). Immunohistochemical study revealed that this antibody successfully reacted with M6b. The specificity of the antibodies were confirmed by imunohistochemistry on the *M6a*-/- or *M6b*-/- brain sections (Fig.1A, B). Coronal sections of mouse brain were prepared, and axon tracts on the each brain sections were identified by mouse brain atlas. Using the newly produced M6b-

specific antibody as well as the previously characterized M6a-specific antibody, I stained wild type mouse brains at three different developmental stages that were E14.5, E16.5 and P0 (Fig.1, 2, 3).

At E14.5, M6a antibody stained the growing axon tracts (Fig.1 C-H). M6a was expressed on the olfactory tract (OT), corticothalamas (CT) and thalamocortical tract (TT). At this stage, CC has not been connected yet. M6b was not detectable at this stage.

At E16.5, as developing proceeds, the major axon tract were more obvious than at E14.5. M6a was expressed on these developing major tracts, including OT, CT, TT, CC and the anterior commissure (AC). At this stage, M6b expression was observed. M6b was also expressed on the developing tract, well overlapping pattern of M6a.

At P0, M6a was expressed on CC, CT, TC and AC that were extensively developing at this stage. M6b was also expressed on these major tract, showing overlapping pattern of M6a.

From E14 to P0, M6a protein was detected mainly in the axon tracts including OT, CC, CT, TC and AC that are the major tract of the brain. At P3 or after this stage, presumably because of the myelination of the axons, M6a and M6b were hardly detectable in the axon tracts, but clearly expressed in the dendrite.

M6a was expressed mainly in growing axons as previously reported (Yan et al., 1993). The newly produced anti-M6b antibody revealed that M6b was well co-localized with

M6a in these axons. The expression of M6b was not detectable at E14.5, and subsequently detectable at E16.5 and P0, displaying comparable overlapping patterns with M6a. In each stages, M6a and M6b proteins were hardly detected in the cell bodies. Although the expressions of M6a and M6b were mostly overlapped in the brain, their expressions in the choroid plexus exhibited different patterns (Fig.1E, 2L, 3B); M6a was strongly expressed along the periphery of the choroid plexus, whereas M6b was mainly expressed the inner region of the choroid plexus.

Confirming similar expression pattern of M6a and M6b in vivo, next I investigated expression pattern of M6 proteins in the subcellular level.

Colocalization of M6a and M6b proteins in the growth cone

I next examined the subcellular distribution of M6 proteins in dissociated neuron culture. Because M6a and M6b were expressed on the olfactory tract, I used culture system of olfactory bulb neuron. To investigate expression pattern of M6a and M6b in vitro, same antibodies used in vivo experiment were used. As described previously, M6a protein was enriched in the edge of growth cones and the shaft of axons in cultured olfactory neurons (Fig.4A). M6b protein exhibited similar distribution (Fig 4A', 4A"). Therefore, I found that M6a and M6b were colocalized in the sub cellular level as well.

Previous studies have shown that binding of anti-M6a antibodies to M6a on growing axons induces aggregation of the protein and redistributes it over the growth cone

membrane, More specifically, after the binding of the antibodies, M6a proteins are stripped off from the growth cone edge and reassembled at the neck of the growth cone. I found that during this reaction, M6b proteins also change the distribution to the growth cone neck together with M6a proteins (Fig 4B', 4B"). Because the anti-M6a antibody does not bind to M6b protein, the redistribution of M6b proteins cannot be due to the direction action of the antibody. Instead, M6b proteins might accompany M6a proteins when they change the location upon bound by the anti-M6a antibody. M6a proteins are oligomerized in the cell membrane (Hirata, unpublished), Therefore, a potential mechanism is that M6a and M6b make heteromeric complexes, which are coclustered by the antibody over the growth cone membrane. Regardless of the mechanisms, however, my observation clearly showed that M6a and M6b are colocalized and behave together, supporting the idea that these proteins function redundantly.

Normal appearance of axon projections in the *M6a*-/- or *M6b*-/- single knockout mice

I next studied the brain morphology of M6 mutant mice. To start with, I analyzed the overall brain structure of the M6a and M6b single mutant mice from E16.5 to Adult. The major axon tracts including OT, CC, CT, TC and AC were basically preserved in the *M6a*-/- single (Fig. 5A, B) and the *M6b*-/- single mutant mice.

Impairment of the CC in the *M6a-/- M6b-/-* double knockout mice

Because the redundant functions for M6a and M6b were postulated, I examined phenotypes of the *M6a-/- M6b-/-* double knockout mice. To obtain *M6a* and *M6b* double knockout mice, *M6a +/- M6b+/-* or *M6a-/- M6b-/-* female mice were mated with *M6a+/- M6b-/Y* or *M6a-/- M6b-/Y* male mice. The double knockout mice were viable and fertile. Because *M6b* gene is located on the Y chromosome, I obtained two patterns of double mutant mice; *M6a-/- M6b-/-* female mice and *M6a-/- M6b-/Y* male mice. I used both types of mice indiscriminately. From now, I recall *M6a-/-M6b-/-* double mutant as a group of the both types of mutants.

Histological analyses of the brain sections revealed that the major axon tracts were present in the double mutants (Fig.5). However, several tracts appeared thinner, compared with those of the wildtype mice. In particular, the CC, the largest axon bundle connecting left and right hemispheres, was clearly hypoplastic in the double mutant at P7 (Fig. 6). The intermediate zone of the neocortex, through which thalamocortical and corticothalamic axons course, was also thinner in *M6a-/-M6b-/-* double mutant mice (Fig 6A, 6B).

To evaluate genotypic influences, I quantified the size of the CC in wildtype, the single and the double mutant mice at P7 (Fig.8). In the double mutant mice, the CC seemed to be smaller along both the anteroposterior and dorsoventral axes. Therefore, I made sagittal sections at the midline of brains, which reflected both dorsoventral and anteroposterior

dimensions of the CC, and measured the area sizes. The average area size of the CC in the *M6a*-/-*M6b*-/- double mutant mice was 40% smaller than that in the wildtype mice (Fig.8D).

Although histological inspections did not lead to an obvious defect in the single homozygous mutants, the quantification indicated that both of the *M6a*-/- *M6b*+/+ and *M6a*+/+ *M6b*-/- single mutant mice, in fact, had the slightly smaller CC. There was no statistical difference in the sizes between the two single mutants. Compared with the mild phenotypes exhibited by the single mutants, the CC hypoplasia in the *M6a*-/- *M6b*-/- double mutants was severer, indicating that functions of M6a and M6b were actually quantitatively additive in formation of the CC.

Developmentally, the callosal axons begin to project around E17, and the CC becomes visible in the mouse brain from E18 (Fame et al., 2011). In these early developmental stages by P0, the CC in the double mutants was not clearly defective (Fig 5C), suggesting that the initial projection of callosal axons is relatively normal in the mutants. However, the defect became obvious by P7. The fully matured brains of the adult double mutant mice still had the thinner CC bundles (Fig.7), indicating that the defective CC in the double mutants is not simply due to a delay of the development. The observations, taken together, suggested that the later projecting callosal axons through P0 and P7 are defective in the mutants.

Although M6a and M6b were expressed major tracts including OT, CC, CT, TC and AC, not all the major axon tracts were defective as CC in the mutants. When I measured the

area size of the AC, which is another callosal tract connecting two hemispheres at the ventral side, the average area sizes were not significantly different among wildtype, *M6a*-/- *M6b*+/+, *M6a*+/+ *M6b*-/- and *M6a*-/- *M6b*-/- mutant mice (Fig.8C,8E).

So far, I found CC formation was defective in *M6a*-/- *M6b*-/- double mouse brain. Then I investigated the cause of this defect based on three possible hypothesis and studied the role of M6 proteins in vivo.

Potential explanations for the CC hypoplasia in the mutants

There are three possibilities that explain the smaller CC bundles in the *M6a*-/- *M6b*-/- mutant brains. 1) The number of the callosal cortical neurons that construct the CC might be reduced. 2) The axons of the callosal neurons might be misguided and deviate from the CC pathway. 3) The axon outgrowth might be impaired in individual callosal neurons. I examined these possibilities one by one.

The normal cell density and layer formation in the mutant neocortex

First, I examined the possibility that the density of cortical neurons was reduced in *M6a*-/- *M6b*-/-. The callosal neurons that construct the CC are positioned in the layer II/III and layer V of the neocortex (Fame et al., 2011). The *M6a*-/- *M6b*-/- showed no apparent abnormalities in the layer structure. Because the cell densities of cortical neurons greatly differ among the layers and

the cortical area, it was essential that picking up same layer of the same cortical area to compare wildtype and mutants. I used mouse brain atlas and carefully picked up cortical layers II/III, IV, V and V of the motor, somatosensory and visual areas and measured the cell density in each layers. In most of these examined categories, the cell density of the *M6a*-/- *M6b*-/- neocortex was comparable with that of the wild-type neocortex (Fig.9). More specifically, the categories containing the callosally projecting CC neurons, which are layer II/III and layer V neurons in the motor and somatosensory areas, exhibited equivalent cell densities between the mutant and wildtype mice (Fig.9 C). There was a slight reduction in the density in the visual cortex of the double mutant. However, these layer IV and VI neurons are not normally implicated in the CC projection, and therefore this difference probably does not contribute to the defect in the CC of the mutant. The layer V neurons in visual area contribute to the CC pojection, but the reduction of the cell density of these neurons was only subtle (wildtype: 15.94±0.88, *M6a*-/- *M6b*-/-: 13.72±0.44) In sum, the results did not support the first possibility that the number of the callosal cortical neurons is reduced in the mutant.

Abnormal callosal pathfinding in the *M6a*-/- *M6b*-/- mutant cortex

Previous studies show several knockout mice for the axon guidance-related genes have phenotype of the defect in the CC formation. For example, the knockout for netrin-1, an axon guidance molecule, completely lacks the CC. In the netrin-1 mutants, the CC axons ectopically

project and terminate near the midline, making an abnormal assembly of the axons called Probst's bundle (Ren 2007). The Probst's bundle is a common feature seen in most of the CC-defective animals including knockout mice for Fgfr-1 or Mena (Smith 2006, Lanier 1999). When the axons fail to sense the midline guidance signals, they probably meander together and are aggregated just before midline.

To follow trajectories of the prospective CC axons, We labeled cortical neurons by electroporating GFP-expression vector into the cortex at E15.5. During this stage, most of the II/III layer neurons are born and therefore selectively incorporate the GFP-expression vector. Because the II/III layer neurons constitute 80% of the mature CC bundle, We expected that this procedure selectively labeled cortical callosal neurons with GFP. Subsequently, the axonal projections of the GFP-labeled neurons were examined at P7.

In the wildtype brain, a cluster of callosal neurons were labeled by GFP, and CC tract was visualized. The projection of the callosal neuron starts from the cortical plate down toward the white matter, then makes a sharp turn to the midline. Crossing midline, the axon again turns to innervate into the cortical plate of the other side. The positions of the cell body of the callosal neuron and its target in the other hemisphere are arranged in a symmetric manner.

Next, I investigated the double mutant brain with GFP-labeled callosal neurons. Consistent with the histological observation, this labeling showed that the number of mid-line crossing axons was smaller in the mutant (Fig.10). However, these axons did not make

a Probst's bundle like the mutant mice of other axon guidance molecules. A closer look revealed that a few prospective CC axons miss-projected into the ipsilateral ventral region in the *M6a*-/- *M6b*-/- mutant (Fig 10). The data indicate that at least some *M6a*-/- *M6b*-/- callosal neurons failed to innervate the normal callosal targets and mis-projected into the striatum.

After I compared the pathway of wildtype and double mutant, I found that significantly smaller number of axons reached to the contralateral cortex in the double mutant. Also, there were ectopic bundles of axons coursing ventrally toward the striatum region in the double mutant. However, this method labeled too many neurons so I could not discriminate and trace one neuron from the cell body to the axon. There was possibility that I labeled the neurons located lateral side of the callosal neurons and normally project into the striatum as well.

To exclude this possibility, next I used single cell labeling system, which labeled callosal neurons sparsely enough to trace one neuron from cell body to the destination. More detailed observations by single cell labeling confirmed the ectopic projections to the striatum indeed originated from the cell bodies in the position specified for the callosal neurons (Fig. 11-14). The plasmid for the single labeling successfully labeled the axons and dendrites of the cortical neurons with the low density enough to discriminate the neurites of each neuron. To trace the projection of each axon from the cell body, I took the images of 100 μm section of the brains using a confocal microscopy, and reconstituted the images of 12 to 15 sections. Then, I obtained the tracing of the cortical axons from one cell body.

In the wildtype, the projections of the CC to the contralateral cortex were traced (Fig.14), and the cell bodies of these axons were located in the layer II/III in the cortex. In two cases, the axons branched and penetrated into the cortex after they reached to the contralateral side, showing normal projection of the CC. On the other hand, in the *M6a*-/- *M6b*-/- mice, there was no projection with midline crossing. Some axons turned toward the midline, however, these axons did not reached the contralateral side (Fig.15A, 15B). These axons were shorter than the widtype, did not have enough length to reach out the midline. Also, there were projection toward lateral side (Fig15C, D, E), and two projections were penetrated into the striatum (Fig.15D, E). These results suggest that at least some callosal axons were misdirected from callosal pathway in the double knockout mice.

I confirmed that these ectopic projections of double mutant to the striatum indeed originated from the cell bodies in the position specified for the callosal neurons. The results suggest that at least some callosal axons were misdirected from callosal pathway in the double knockout mice. Therefore, the possibility "2) The axons of the callosal neurons are misdirected from callosal pathway" was indeed the one of the cause of the defect of CC in the double mutant.

Cell-autonomous impairment of axon growth in *M6a*-/- *M6b*-/- neurons

Although the axon labeling analysis revealed mis-projection of some cortical callosal axons, this

anomaly appeared rather minor. The most notable difference detected by the analysis was that the far smaller number of GFP-labeled axons grew long in the mutant neocortex (Fig.10). Eventually, fewer axons reached to the contralateral side through the CC. Furthermore, even the axons that successfully reached the contralateral side, they rarely gave off the collateral branches that penetrated into the contralateral cortical plate. Therefore, the cortical callosal neurons in the double mutants resulted in few GFP-labeled axons in the their normal target, the contralateral cortical plate.

If cortical callosal neurons were incapable of extending a sufficient length of axons, the axons would not reach the midline, making the CC bundle size smaller. To address this possibility, I used in vitro system. I cultured wild type and *M6a*-/- *M6b*-/- cortical neurons and compared the neurite development. In this analysis, I roughly discriminated layer II/III neurons and the other layer neurons by injecting BrdU at E16 when most of the layer II/III neurons are born. BrdU-positive and negative neurons were discriminated by immunostaining after neurons were cultured. Cells with BrdU incorporated nuclei were detected by anti-BrdU antibody after DNA denaturing.

In the wildtype, the expression pattern of M6a and M6b in the cortical neurons were investigated. Both the BrdU-positive and negative populations, M6a and M6b were expressed abundantly in axons and minor processes including their growth cones.

Next, I quantify the length of axonal length of the cortical neurons in the wild

type and mutants. The quantification indicated that the axonal length extended from the single and double mutant neurons was significantly smaller than that from wildtype neurons (Fig.13B). There was no statistical significance in the average length between each single and the double mutant neurons. The length of the dendrites of *M6a*-/- *M6b*-/- neurons was also significantly smaller than that of wild-type neurons (Fig.13C). This impairment in neurite outgrowth was similarly observed for the BrdU-positive layer II/III neurons and BrdU-negative other layer neurons, suggesting that the defect was not limited to the layer II/III neurons, but rather common to all layer neurons (Fig.13D, E, F). Taken together, the analysis indicated that *M6a* and *M6b* mutant cortical neurons are cell autonomously defective for the neurite outgrowth.

Although both of the axons and dendrites were affected by the mutation, the mutant neurons still maintained the normally polarized morphology with a single axon and multiple dendrites. Furthermore, wildtype and the mutant neurons had a similar number of dendrites and axon branches.

The rescue experiment of impaired neurite outgrowth in the double mutant neurons by introducing M6 proteins

I attempted to rescue the reduced neurite outgrowth of the double mutant neurons by introducing M6 protein members. Plasmids encoding GFP-tagged M6a, M6b and DM20 were transfected into the cortical neurons of the *M6a*-/- *M6b*-/- by in utero electroporation, and the neurons were

then dissociated and cultured (Fig14A). The normal neurite length was restored in the neurons when they were supplemented with any one of the proteins (Fig.14C). These results suggest that M6a and M6b proteins have redundant functions in the neurite outgrowth and that the expression of any one of them is sufficient to rescue the neurite outgrowth of cortical neurons to the normal level. Moreover, although DM20 is hardly expressed in neurons, this oligodendrocytic protein can have same function of M6a and M6b proteins when it is force-expressed in the neurons.

Effect of M6a over-expression on the wild type neuron

I also expressed M6a protein in the wild-type cortical neurons to examine whether the over-expression further enhanced the neurite outgrowth. However, M6a did not enhance the neurite outgrowth beyond the normal wild-type level (Fig.14B). This suggests that there is a critical amount of M6 proteins that is required for the normal axonal outgrowth.

Mapping the functional domain of M6a for the axonal outgrowth

Using culture system, I attempted to map the functional domain of M6a that was required for the axonal growth. The M6a cDNA expression plasmids for the deletion constructs were transfected into cortical neurons of the *M6a*-/- *M6b*-/- double mutant. The transfection of the mutant constructs lacking either N-terminal (M6a Δ1-25) or C-terminal intracellular domain (M6a Δ238-278) restored the neurite length to the normal level (Fig.14D, E). On the other hands, the

deletion construct of the second intracellular domain did not restore the neurite length. The deletion of the complete second intracellular domain (IC2, Δ105-128) did not rescued the impaired neurite length of the double knockout mice. To narrow the range of the required domain in the second intracellular loop, the deletion of the first half and second half of IC2 (Δ105-114 and Δ115-128) were introduced into the double knockout mice neuron. However, neither of the constructs rescued the axonal length of double knockout mice cortical neurons, suggesting that both domains in IC2 region are required for the proper axonal growth (Fig.14D, E). In summary, I found that the second intracelular loop (M6a Δ105-128) were required for restoration of the axonal length, but not the N- and C-terminus.

Development of the CC in the *M6a-/- M6b-/Y PLP-/Y* triple knockout mice

Although PLP/DM20 has been believed as the main component of the myelin and solely expressed by oligodendrocytes, a recent study reports neuronal expression of a splicing isoform of PLP/DM20 in neurons (Miller 2009). To evaluate the contribution of PLP/DM20 in formation of the CC bundle, we made *M6a-/- M6b-/Y PLP-/Y* triple knockout mice. Because *M6b* and *PLP* were both positioned in the X chromosome, it was not easy to make the *M6b* and *PLP* double mutants. By crossing *M6b-/-* female and *PLP-/Y* male mice, I occasionally obtained the mutant mice with a recombined X chromosome that has both of the mutations together. The mutants, however, developed a severe demyelination phenotypes (unpublished by Dr, Hauke and Nave)

by two month of age, and were not be able to be used for the further mating. Therefore, to obtain the *M6a-/- M6b-/Y PLP-/Y* triple embryos, I mated *M6a-/- M6b+/- PLP+/-* female with *M6a-/-* male mice and waited for a random recombination between the *M6b* and *PLP* loci.

From the 45 crossings, I successfully obtained four triple mutants, which were three embryos at E18.5 and one adult at P90. The major axon tracts were still present in the *M6a-/- M6b-/Y PLP-/Y* triple mutant at E18.5 (Fig.5D). Although limitation of the number of the triple mutants did not allow a quantitative analysis of the CC size, the sizes of the triple and double mutants appeared comparable at the stage of E18.5. The adult *M6a-/- M6b-/Y PLP-/Y* triple mouse also had a similarly sized CC to that of the *M6a-/- M6b-/-* double mutant (Fig.7E, 7F, 7I). The results indicated the *M6a-/- M6b-/Y PLP-/Y* triple mutants are still capable of connecting the two hemisphere of the cortex via the CC.

Discussion

In this study, I showed the malformation of CC in the *M6a*-/- *M6b*-/- mutant mice. I also demonstrated that two possible causes for this abnormality; one is the ectopic projection from the callosal neurons into the striatum ; the other is impairment of axonal growth in individual callosal neurons. The evidence for the former phenotype was obtained in GFP labeling of the callosal axons, which make ectopic bundles coursing ventrally toward the striatum only in the *M6a*-/- *M6b*-/- mice. Single cell labeling confirmed that these ectopic projections to the striatum originate from the cell bodies in the layer II/III, where the callosal neurons are normallly positioned. On the other hand, the latter evidence was obtained from primary cultured neurons. When the cortical neurons of the *M6a*-/- *M6b*-/- were cultured, their neurite length was significantly shorter than that of wild-type neurons. This neurite growth impairment was rescued by the forced expression of M6 proteins in the double mutant cortical neurons. These results confirmed that the reduced axonal growth in the *M6a*-/- *M6b*-/- mice was indeed caused by the absence of M6 proteins. Finally, we found that the second intracellular loop of M6a was required for the normal axonal growth.

In the present study, the callosal neurons were shorter and also ectopically projected in the *M6a*-/- *M6b*-/- mice. It is still unclear that whether these two phenotype; the misrouting projection and the impaired axonal growth are related or not. There is a possible

hypothesis assuming that the two phenotype are related to each other. The misrouting projection may occur as a consequence of impaired axonal outgrowth. In the callosal projection, the axons proceed through the environment which is abundant with lots of guidance molecules. The pattern of these molecules changes over time to contribute to selective axonal guidance. The axons are required to reach precise position with precise timing. In M6 mutants, because the length of callosal axons are impaired, the axons might not reach to proper positions to access to the proper axon guidance molecules. In this case, the ectopic projection phenotype may be regarded as the result of the impaired axonal length.

Redundant function of the M6 proteins

I speculated that M6a and M6b proteins have redundant function because they show high similarity. This speculation was supported by the following three observations in this study. First, M6a and M6b were well co-localized in vivo. More specifically, M6a and M6b were both expressed in the major tracts at E16.5 and P0 with an overlapping manner. In the cultured olfactory bulb neurons, M6a and M6b were both distributed in the edge of the growth cone and the shaft fillopodia, suggesting the intimate molecular interaction at the subcellular level. Second, the impairment of CC was much more significant in the *M6a*-/- *M6b*-/- double knockout mice than the *M6a*-/- or *M6b*-/- single mice. The reduction in the average size of the CC in the *M6a*-/- *M6b*-/- double knockout mice was about the same as the sum of the reduction in each

single knockout mice, suggesting that M6a and M6b have actually simple additive functions in vivo. Third, in the culture, the impairment of the axonal growth in the *M6a*-/- *M6b*-/- double knockout neurons was restored by the expression of either M6a or M6b. This suggests that M6a and M6b can play equivalent molecular function in the axonal growth. Probably, the total amount of M6a plus M6b matters more than the amount of each one of the proteins, Taken together, our results did not support the idea of two different functions specific to individual M6a proteins but suggested their shared common function in the axon outgrowth.

Other molecules associated with the CC formation

Many molecules regulate the midline crossing and targeting of callosal axons (Donahoo et al., 2009). Mammalian Enabled (Mena) and Growth-Associated Protein-43 (GAD-43) plays a role in actin cytoskeleton dynamics and modulates actin polymerization at the tip of the growth cone filopodia (Lanier et al., 1999; Shen et al., 2002). Also, microtuble-associated proteins (MAPs) stabilize microtubules at the growth cone to maintain its motility (Takei et al., 2000; Teng et al., 2001). When these genes are disrupted in mice, the callosal axons do not cross the midline and make a prominent Probost's bundle in the ipsilateral side. Similar callosal axon phenotypes have been reported in knockout mice for various axon guidance molecules and their receptor molecules. Long-range axon guidance signals through Slit/Robo play critical roles in axon guidance across the midline crossing (Shu et al., 2003; López -Bendito et al., 2007; Andrews et

al., 2006; Sundaresan et al., 2004; Bagri et al., 2002). Wnt5a is necessary for the CC formation through Frizzled3-mediated and Receptor-like Tyrosine kinase (Ryk)-mediated signaling (Keeble et al., 2006; Wang et al., 2006; Li et al 2009). In addition, Netrin1/DCC signals are also required for the CC formation (Serafini et al., 1996; Fazeli et al., 1997; Ren et al., 2007). Multiple class 3 Semaphorins (Sema3) are involved in the guidance of the CC axons through the Neuropilin (Nrp) receptors (Niquille et al., 2009 Hatanaka et al., 2009; Piper et al., 2009; Zhao et al., 2011). Short-range guidance molecules such as ephrins and EphA5, EphB1 and EphrinB3 are also essential for CC formation (Hu et al., 2003; Mendes et al., 2006). These many observations support the idea that the midline crossing of the callosal axons is intricately and sequentially regulated by multiple different axon guidance signals. It is of note that knockout mice for all these guidance signals develop the CC malformation with the characteristic axonal misrouting, called Probst's bundle. However, knockout mice for M6 did not exhibit a phenotype involving Probst's bundle. Therefore, M6 proteins may not be directly linked with the above-mentioned known guidance systems that work in the CC formation.

A different type of the CC abnormality has been reported in the knockout mice for transcription factor Satb2. Satb2 is necessary for specification of the callosal neurons through repression of COUPTF interacting protein 2 (CTIP2), another transcription factor critical for specification of corticofugal projecting neurons. In the absence of Satb2, callosal neurons change the fate to corticofugal projecting neurons and extend their axon subcortically,

through the internal capsule. Thus, the size of the anterior comissure increased instead of CC (Alcamo et al., 2008; Britanova et al., 2008). Indeed, by the single cell tracing, there were misrouting population in the double knockouts. Some axons projecting lateral direction to the ventral side, whereases the size of the anterior comissure did not increased, rather slightly decreased. Taking together, this misrouting phenotype of the Satb2 mutant is also different from that of the M6 knockout mice observed in this study.

Functional domains of M6a for the axonal growth

Previous study showed that the over-expression of M6a enhanced the formation of membrane protrusions (Sato et al., 2011b) and filopodia/spine (Alfonso et al., 2005; Brocco et al., 2010). For the formation of membrane protrusions, the N-terminus domain (amino acid 1-62) of M6a is required (Sato et al., 2011b). For the formation of filopodia/spine, the second extracellular domain (C174 and C192) is essential (Fuchsova et al., 2009). When the anti-M6a antibody stalls axon alongation, a short N-terminus sequence (amino acid 1-25) is important (Sato et al., 2011a). None of these M6a domains reported previously have an overlap with the second intracellular loop (amino acid 105-128) identified in this study. This second intracellular domain required for axonal growth includes two cysteine residues (C122 C125) that are potential targets of palmitoylation. Because the palmitoylation in some four-transmembrane proteins is implicated in

molecular-molecular interactions across the cell membrane (Stipp et al., 2003), such modification of this M6a domain could have a similar functional significance. The axon growth requires various cytosolic and cytoskeltal molecules. It is interesting to know whether the second intracellular loop identified in this study interacts with some of these molecules that regulate axonal elongation.

The relationship between the axon growth arrest by anti-M6a antibody and the impaired axonal outgrowth in M6 mutants

Anti-M6a antibody inhibits the axon outgrowth. This axon-growth inhibition induced by the antibody binding is much more dramatic than that by simple elimination of M6a in cultured neurons, leading to the idea that the anti-M6a antibody positively induces an axon stalling reaction but not simply inhibits the function of M6a (Sato et al., 2011a). However, there was a pitfall in this argument. As I showed in this study, anti-M6a antibody affected not only M6a but also M6b indirectly, although the antibody does not directly bind to M6b. Therefore, the action of antibody in the previous study could have involved both M6a and M6b, and may not be appropriate to be compared with the situation of neurons that lack only M6a. Based on the results of this study, I can address this argument. Although the axon growth of the *M6a*-/- *M6b*-/- double knockout neurons was significantly impaired, this impairment was still moderate comparing with the drastic inhibition of axon outgrowth by the anti-M6a antibody. Furthermore,

as described before, the stalling reaction induced by the antibody required the different domains of M6a from the efficient axonal growth. These results indicate that the anti-M6a antibody does not inhibit the function of M6a or M6b, but positively stops the axonal elongation.

Then, how is the axon growth is inhibited by the anti-M6a antibody? I will discuss two possible mechanisms here. First is the structural change of the membrane. With the antibody binding, the M6a proteins were reassembled at the neck of the growth cone with M6b proteins. Because of the aggregation of the membrane proteins, the flexibility of membrane at the tip of the growing axon might be affected physically. This change of membrane structure might inhibit the normal movement of the growth cone and cause the stalling of the axon. Second, the aggregation of M6a and M6b proteins by the antibody could also capture other axonal growth-related molecules. M6a interacts with G protein-coupled μ-opioid receptor at the transmembrane domain and regulate its membrane recycling (Wu et al., 2007; Liang et al., 2008). M6b interacts with the serotonin transporter and promote its expression on the cell surface (Fjorback et al., 2009). If M6 proteins interact with molecules that function for axonal growth, their co-aggregation by the anti-M6a antibody might severely affect the subsequent axon outgrowth.

Function of PLP/DM20 protein in the CC formation

I generated *M6a-/- M6b-/Y PLP-/Y triple* knockout mice to evaluate possible redundant function of PLP/DM20 in the CC formation. However, *M6a-/- M6b-/Y PLP-/Y* did not develop further

impairment in the CC beyond the *M6a-/- M6b-/-* double mutant. Therefore, PLP/DM20 does not seem to function redundantly with M6a or M6b in the CC formation. However, because PLP/DM20 rescued the impaired axon growth in the *M6a-/- M6b-/-* double mutant, this protein itself should have a similar function to M6a and M6b at the molecular level. There is also evidence that PLP/DM20 and M6b function redundantly in myelination by oligodendrocytes (Dr. Werner and Nave, unpublished observation). I assume that the seeming non-redundant function of PLP/DM20 in the CC is due to its distinct expression patterns in neurons. Previous studies have shown that PLP/DM20 is predominately expressed in oligodendrocytes. Although resent studies revealed that a splicing isoform of PLP/DM20 (sr-PLP/sr-DM20) is expressed in the mouse cortical neuron from E13 to P7 (Jacobs et al., 2003; Miller et al., 2009), anti- sr-PLP/DM20 antibody did not label axon tracts. The authors discussed that localization of this neuronal isoform is subcellularly restricted to the cell body of neurons. Therefore, distribution of PLP/DM20 protein in neurons is quite dissimilar from that of M6a and M6b, and could be the reason why we did not detect an additive phenotype in the CC of the *M6a-/- M6b-/Y PLP-/Y* triple knockout mice.

Summary

In this study, I showed that M6 proteins have an essential role in the formation of the CC by regulating the axonal growth of callosal neurons. M6a and M6b are functionally redundant in this process. Based on the results from the primary cultured neurons, the defect of the CC in the *M6a*-/- *M6b*-/- double knockout mice is at least partly due to the reduced length of axons, which can be attributed to the impairment in the intrinsic ability of individual callosal neurons to extend the sufficient length of axons. Furthermore, the study revealed that some callosal axons are misguided ventrally in the double knockout mice, which should also contribute to the hypoplasia in the CC.

Acknowledgements

I thank Dr.Yumiko Saga for constructing M6a KO mouse, Drs.Klaus-Armin Nave and Hauke Werner for M6b KO mouse, Dr.Hidenobu Mizuno for in utero electroporation. Ms. Noriko Yamauchi, Kazue Abe and Norie Yamane for technical assistance, and I thank Dr.Tatsumi Hirata, and all other members of Hirata lab for helpful discussion and heartful encouragement.

References

Alcamo, E.A., Chirivella, L., Dautzenberg, M., Dobreva, G., Fariñas, I., Grosschedl, R., McConnell, S.K. (2008) Satb2 regulates callosal projection neuron identity in the developing cerebral cortex. Neuron 57: 364-377.

Alfonso, J., Fernandez, M.E., Cooper, B., Flugge, G., Frasch, A.C. (2005) The stress-regulated protein M6a is a key modulator for neurite outgrowth and filopodium/spine formation. Proc Natl Acad Sci U S A 102: 17196-17201.

Andrews, W., Liapi, A., Plachez, C., Camurri, L., Zhang, J., Mori, S., Murakami, F., Parnavelas, J.G., Sundaresan, V., Richards, L.J. (2006) Robo1 regulates the development of major axon tracts and interneuron migration in the forebrain. Development 133: 2243-2252.

Bagri, A., Marín, O., Plump, A.S., Mak, J., Pleasure, S.J., Rubenstein, J.L., Tessier-Lavigne, M. (2002) Slit proteins prevent midline crossing and determine the dorsoventral position of major axonal pathways in the mammalian forebrain. Neuron 33: 233-248.

Baumrind, N.L., Parkinson, D., Wayne, D.B., Heuser, J.E., Pearlman, A.L. (1992) EMA: a

developmentally regulated cell-surface glycoprotein of CNS neurons that is concentrated at the leading edge of growth cones. Dev. Dyn. 194: 311-325.

Britanova, O., de Juan, Romero. C., Cheung, A., Kwan, K.Y., Schwark, M., Gyorgy, A., Vogel, T., Akopov, S., Mitkovski, M., Agoston, D., Sestan, N., Molnár, Z., Tarabykin, V. (2008) Satb2 is a postmitotic determinant for upper-layer neuron specification in the neocortex. Neuron 57: 378-392.

Brocco, M.A., Fernández, M.E., Frasch, A.C. (2010) Filopodial protrusions induced by glycoprotein M6a exhibit high motility and aids synapse formation. Eur. J. Neurosci. 31: 195-202.

Cooper, B., Werner, H.B., Flügge, G. (2008) Glycoprotein M6a is present in glutamatergic axons in adult rat forebrain and cerebellum. Brain. Res. 1197: 1-12.

Donahoo, A.L., Richards, L.J. (2009) Understanding the mechanisms of callosal development through the use of transgenic mouse models. Semin. Pediatr. Neurol. 16: 127-142.

Fame, R.M., MacDonald, J.L., Macklis, J.D. (2011) Development, specification, and diversity of

callosal projection neurons. Trends. Neurosci. 34: 41-50.

Fazeli, A., Dickinson, S.L., Hermiston, M.L., Tighe, R.V., Steen, R.G., Small, C.G., Stoeckli, E.T., Keino-Masu, K., Masu, M., Rayburn, H., Simons, J., Bronson, R.T., Gordon, J.I.,Tessier-Lavigne, M., Weinberg, R.A. (1997) Phenotype of mice lacking functional Deleted in colorectal cancer (Dcc) gene. Nature 386: 796-804.

Fjorback, A.W., Müller, H.K., Wiborg, O. (2009) Membrane glycoprotein M6B interacts with the human serotonin transporter. J. Mol. Neurosci. 37: 191-200.

Fuchsova, B., Fernández, M.E., Alfonso, J., Frasch, A.C. (2009) Cysteine residues in the large extracellular loop (EC2) are essential for the function of the stress-regulated glycoprotein M6a. J. Biol. Chem. 284: 32075-32088.

Garcez, P.P., Henrique, N.P., Furtado, D.A., Bolz, J., Lent, R., Uziel, D. (2007) Axons of callosal neurons bifurcate transiently at the white matter before consolidating an interhemispheric projection. Eur. J. Neurosci. 25: 1384-1394.

Hatanaka, Y., Matsumoto, T., Yanagawa, Y., Fujisawa, H., Murakami, F., Masu, M. (2009)

Distinct roles of neuropilin 1 signaling for radial and tangential extension of callosal axons. J. Comp. Neurol. 514: 215-225.

Hu, Z., Yue, X., Shi, G., Yue, Y., Crockett, D.P., Blair-Flynn, J., Reuhl, K., Tessarollo, L., Zhou, R. (2003) Corpus callosum deficiency in transgenic mice expressing a truncated ephrin-A receptor. J. Neurosci. 23: 10963-10970.

Jacobs, E.C., Bongarzone, E.R., Campagnoni, C.W., Kampf, K., Campagnoni, A.T. (2003) Soma-restricted products of the myelin proteolipid gene are expressed primarily in neurons in the developing mouse nervous system. Dev. Neurosci. 25: 96-104.

Keeble, T.R., Halford, M.M., Seaman, C., Kee, N., Macheda, M., Anderson, R.B., Stacker, S.A., Cooper, H.M. (2006) The Wnt receptor Ryk is required for Wnt5a-mediated axon guidance on the contralateral side of the corpus callosum. J. Neurosci. 26: 5840-5848.

Kitagawa, K., Sinoway, M.P., Yang, C., Gould, R.M., Colman, D.R. (1993) A proteolipid protein gene family: expression in sharks and rays and possible evolution from an ancestral gene encoding a pore-forming polypeptide. Neuron 11: 433-448.

Lagenaur, C., Kunemund, V., Fischer, G., Fushiki, S., Schachner, M. (1992) Monoclonal M6 antibody interferes with neurite extension of cultured neurons. J. Neurobiol. 23: 71-88.

Lanier, L.M., Gates, M.A., Witke, W., Menzies, A.S., Wehman, A.M., Macklis, J.D., Kwiatkowski, D., Soriano, P., Gertler, F.B. (1999) Mena is required for neurulation and commissure formation. Neuron 22: 313-325.

Li, L., Hutchins, B.I., Kalil, K. (2009) Wnt5a induces simultaneous cortical axon outgrowth and repulsive axon guidance through distinct signaling mechanisms. J. Neurosci. 29: 5873-5883.

Liang, Y.J., Wu, D.F., Stumm, R., Hollt, V., Koch, T. (2008) Membrane glycoprotein M6A promotes mu-opioid receptor endocytosis and facilitates receptor sorting into the recycling pathway. Cell. Res. 18: 768-779.

Livy, D.J., Schalomon, P.M., Roy, M., Zacharias, M.C., Pimenta, J., Lent, R., Wahlsten, D. (1997) Increased axon number in the anterior commissure of mice lacking a corpus callosum. Exp. Neurol. 146: 491-501.

López-Bendito, G., Flames, N., Ma, L., Fouquet, C., Di, Meglio. T., Chedotal, A., Tessier-

Lavigne, M., Marín, O. (2007) Robo1 and Robo2 cooperate to control the guidance of major axonal tracts in the mammalian forebrain. J. Neurosci. 27: 3395-3407.

Mendes, S.W., Henkemeyer, M., Liebl, D.J. (2006) Multiple Eph receptors and B-class ephrins regulate midline crossing of corpus callosum fibers in the developing mouse forebrain. J. Neurosci. 26: 882-892.

Michibata, H., Okuno, T., Konishi, N., Kyono, K., Wakimoto, K., Aoki, K., Kondo, Y., Takata, K., Kitamura, Y., Taniguchi, T. (2009) Human GPM6A is associated with differentiation and neuronal migration of neurons derived from human embryonic stem cells. Stem. Cells. Dev. 18: 629-639.

Miller, M.J., Kangas, C.D., Macklin, W.B. (2009) Neuronal expression of the proteolipid protein gene in the medulla of the mouse. J. Neurosci. Res. 87: 2842-2853.

Mitchell, B.D., Macklis, J.D. (2005) Large-scale maintenance of dual projections by callosal and frontal cortical projection neurons in adult mice. J. Comp. Neurol. 482: 17-32.

Mizuno, H., Hirano, T., Tagawa, Y. (2007) Evidence for activity-dependent cortical wiring:

formation of interhemispheric connections in neonatal mouse visual cortex requires projection neuron activity. J. Neurosci. 27: 6760-6770.

Mizuno, H., Luo, W., Tarusawa, E., Saito, YM., Sato, T., Yoshimura, Y., Itohara, S., Iwasato, T. (2014) NMDAR-regulated dynamics of layer 4 neuronal dendrites during thalamocortical reorganization in neonates. Neuron. 16;82: 365-79

Mukobata, S., Hibino, T., Sugiyama, A., Urano, Y., Inatomi, A., Kanai, Y., Endo, H., Tashiro, F. (2002) M6a acts as a nerve growth factor-gated Ca(2+) channel in neuronal differentiation. Biochem Biophys Res Commun 297:722-728.

Niquille, M., Garel, S., Mann, F., Hornung, J.P., Otsmane, B., Chevalley, S., Parras, C., Guillemot, F., Gaspar, P., Yanagawa, Y., Lebrand, C. (2009) Transient neuronal populations are required to guide callosal axons: a role for semaphorin 3C. PLos. Biol. 7: e1000230.

Piper, M., Plachez, C., Zalucki, O., Fothergill, T., Goudreau, G., Erzurumlu, R., Gu, C., Richards, L.J. (2009) Neuropilin 1-Sema signaling regulates crossing of cingulate pioneering axons during development of the corpus callosum. Cereb. Cortex. 19: i11-i21.

Paul, L.K., Brown, W.S., Adolphs, R., Tyszka, J.M., Richards, L.J., Mukherjee, P., Sherr, E.H. (2007) Agenesis of the corpus callosum: genetic, developmental and functional aspects of connectivity. Nat. Res. Neurosci. 8: 287-299.

Ren, T., Zhang, J., Plachez, C., Mori, S., Richards, L.J. (2007) Diffusion tensor magnetic resonance imaging and tract-tracing analysis of Probst bundle structure in Netrin1- and DCC-deficient mice. J. Neurosci. 27: 10345-10349.

Sato, Y., Mita, S., Fukushima, N., Fujisawa, H., Saga, Y., Hirata, T. (2011a) Induction of axon growth arrest without growth cone collapse through the N-terminal region of four-transmembrane glycoprotein M6a. Dev. Neurobiol. 71: 733-746.

Sato, Y., Watanabe, N., Fukushima, N., Mita, S., Hirata, T. (2011b) Actin-independent behavior and membrane deformation exhibited by the four-transmembrane protein M6a. PLos One 6: e26702.

Serafini, T., Colamarino, S.A., Leonardo, E.D., Wang, H., Beddington, R., Skarnes, W.C., Tessier-Lavigne, M. (1996) Netrin-1 is required for commissural axon guidance in the

developing vertebrate nervous system. Cell 87: 1001-1014.

Shen, Y., Mani, S., Donovan, SL., Schwob, JE., Meiri, KF. (2002) Growth-associated protein-43 is required for commissural axon guidance in the developing vertebrate nervous system. J. Neurosci. 1;22: 239-47

Shu, T., Sundaresan, V., McCarthy, M.M., Richards, L.J. (2003) Slit2 guides both precrossing and postcrossing callosal axons at the midline in vivo. J. Neurosci. 23: 8176-8184.

Sundaresan, V., Mambetisaeva, E., Andrews, W., Annan, A., Knöll, B., Tear, G., Bannister, L. (2004) Dynamic expression patterns of Robo (Robo1 and Robo2) in the developing murine central nervous system. J. Comp. Neurol. 468: 467-481.

Stipp, C.S., Kolesnikova, T.V., Hemler, M.E. (2003) Functional domains in tetraspanin proteins. Trends. Biochem. Sci. 28: 106-112.

Takei, Y., Teng, J., Harada, A., Hirokawa, N. (2000) Defects in axonal elongation and neuronal migration in mice with disrupted tau and map1b genes. J. Cell. Biol. 150: 989-1000.

Teng, J., Takei, Y., Harada, A., Nakata, T., Chen, J., Hirokawa, N. (2001) Synergistic effects of MAP2 and MAP1B knockout in neuronal migration, dendritic outgrowth, and microtubule organization. J. Cell. Biol. 155: 65-76.

Wang, Y., Zhang, J., Mori, S., Nathans, J. (2006) Axonal growth and guidance defects in Frizzled3 knock-out mice: a comparison of diffusion tensor magnetic resonance imaging, neurofilament staining, and genetically directed cell labeling. J. Neurosci. 26: 355-364.

Wu, D.F., Koch, T., Liang, Y.J., Stumm, R., Schulz, S., Schroder, H., Hollt, V. (2007) Membrane glycoprotein M6a interacts with the micro-opioid receptor and facilitates receptor endocytosis and recycling. J. Biol. Chem. 282: 22239-22247.

Yan, Y., Lagenaur, C., Narayanan, V. (1993) Molecular cloning of M6: identification of a PLP/DM20 gene family. Neuron 11: 423-431.

Zhao, H., Maruyama, T., Hattori, Y., Sugo, N., Takamatsu, H., Kumanogoh, A., Shirasaki, R., Yamamoto, N. (2011) A molecular mechanism that regulates medially oriented axonal growth of upper layer neurons in the developing neocortex. J. Comp. Neurol. 519: 834-848.

Zhao, J., Iida, A., Ouchi, Y., Satoh, S., Watanabe, S. (2008) M6a is expressed in the murine neural retina and regulates neurite extension. Mol. Vis. 14: 1623-1630.

Figure legends

Figure 1. Expression of M6a and M6b in the developing mouse brain at E14.5. (A-B) Specificity of anti-M6a and M6b antibody. Exclusive detection of M6b protein in the *M6a*-/- mice (A), and M6a protein in the *M6b*-/- mice (B) at E16.5. (C-H) M6a expression (C-H) and M6b expression (C'-H') in the wildtype mice brains at E14.5. Coronal sections of the brains are alined from anterior to the posterior. (C"-H") shows merged image of M6a (green) and M6b (magenta) expression. M6a was expressed in the growing axon tracts (arrowheads in D-F, arrow in D) whereas, M6b was not detected at this stage. Scale bar, 1000μm.

Figure 2. Expression of M6a and M6b in the developing mouse brain at E16.5. (A-K) M6a expression (A-K) and M6b expression (A'-K') in the wildtype mice brains at E16.5. Coronal sections of the brains are alined from anterior to the posterior. (A"-K") shows merged image of M6a (green) and M6b (magenta) expression. M6a and M6b had overlapped expression pattern and were expressed in the axons tract in the intermediate zone including the thalamocortical, the corticothalamus and the corpus callosum (CC) tracts (arrowheads in B-G) as well as the anterior commissure (AC) tracts (arrows in D). (L-N) (L, M, N) are the magnified images of (C", D", E"), respectively. Scale bars, 500μm.

Figure 3. Expression of M6a and M6b in the developing mouse brain at P0. (A-D) M6a expression (A-D) and M6b expression (A'-D') in the wildtype mice brains at P0. Coronal sections of the brains are alined from anterior to the posterior. (A"-D") shows merged image of M6a (green) and M6b (magenta) expression. M6a and M6b had overlapped expression pattern

and were expressed in the axons tract including the thalamocortical, the corticothalamus and the corpus callosum (CC) tracts (arrowheads in A-C). Scale bar, 500μm.

Figure 4. Distribution of M6 proteins on the culture olfactory bulb (OB) axons. (A) Expression of M6a (A)and M6b (A') in the OB axons. (A") is a merged image of M6a (green) and M6b (magenta). M6a is expressed in the membrane edge of the growth cone and axon shaft (A), with M6b (A', A"). (B) Localization of the M6a (B) in the OB axons treated with mAb M6 for 30 min and then subjected to immunostaining with anti-M6a antibody (MBL). The M6a proteins are stripped off from the growth cone edge and reassembled at the neck of the growth cone (B). M6b proteins also change the distribution to the growth cone neck together with M6a proteins (B'). (B") is a merged image of M6a (green) and M6b (magenta).

Figure 5. Histological comparison of wildtype and mutant brains. (A-D) HE staining of the brain in the wildtype (A), the *M6a*-/- single mutant (B), and the *M6a*-/- *M6b*-/*Y* double mutant (C) at P0. The *M6a*-/- *M6b*-/*Y PLP*-/*Y* triple mutant was delivered by Caesarean section and analyzed at E18.5 (D). Matched sections are alined from the anterior part (A-D), the middle part (A'-D') and the posterior part (A"-D"). The major axon tracts were grossly preserved in the *M6a*-/- single mutant (B), the *M6a*-/- *M6b*-/*Y* double mutant (C), and the *M6a*-/- *M6b*-/*Y PLP*-/*Y* triple mutant (D). At P0, the defect in CC was not obvious in the *M6a*-/- *M6b*-/*Y* double mutant (C), and the *M6a*-/- *M6b*-/*Y PLP*-/*Y* triple mutant (D). Scale bar, 500μm.

Figure 6. Impairment of the CC formation in *M6a*-/- *M6b*-/- knockout mice at P7. (A-D) HE staining of the brain in the *M6a*+/- (A, C) and the *M6a*-/- *M6b*-/*Y* double mutant (B, D) at P7. (C) and (D) are magnified image of the boxes in (A) and (B), respectively, Several tracts in

M6a-/- M6b-/- knockout mice were thinner, in particular, the CC hypoplasia was clear (arrowheads in C and D). (E-F) Neurofilament staining of the CC in the wildtype (E) and the *M6a-/- M6b-/Y* double mutant (F). Although the CC formation was impaired (arrowheads in E and F), the presence of Probst's bundles was not detected. Scale bars, 500μm.

Figure 7. Impairment of the CC formation in mutant adult brains . (A-I) Myelin staining of the wildtype (A, B), and the *M6a-/- M6b-/Y* double mutant (C, D) at P60. The *M6a-/- M6b-/Y PLP-/Y* triple mutant was analyzed at P90 (E, F). (A, C, E) are the anterior part and (B, D, F) are the posterior part of the matched sections. (G), (H), (I) are magnified images of the (A), (C), (E), respectively. The CC were thinner in the *M6a-/- M6b-/Y* (C, D, H) and in the *M6a-/- M6b-/Y PLP-/Y* (E, F, I). The *M6a-/- M6b-/Y PLP-/Y* had the callosal connection (E, F, I). Scale bars, 2.0mm.

Figure 8. Measurement of the CC and the anterior commissure (AC) area sizes. (A-C) Method of the measurement of the CC and AC sizes. Series of the sagittal sections with HE straining were obtained at P7 and the five sections at the midline were selected. The CC area size (the area surrounded by the doted line in B) and the AC area size (the area surrounded by the doted line in C) were measured by the imageJ software, (D-E) The average sizes of the CC (D) and the AC (E) of *M6a+/-, M6a-/-, M6b-/-* and *M6a-/- M6b-/-* brain at P7. In the *M6a+/-* and *M6a-/- M6b-/-*, the area size of the CC was significantly different ($*$ $p<0.05$ by multiple comparison of Tukey's test), whereas, *M6a-/-* and *M6b-/-* single knockout mice did not show the significant difference with neither *M6a+/-* nor *M6a-/- M6b-/-*. The area size of the AC was not significantly different in any mutants. Scale bars, 500μm.

Figure 9. Normal cell density and layer formation in the mutant neocortex. (A-B) Method of the measurement of the cell density. the coronal section with NeuN (neuron marker) staining were obtained at P7. The number of NeuN positive neurons per 50x200μm square was measured (A). The cell density in each layer of the motor, somatosensory and visual cortical areas were determined by mouse P6 and adult atlas(B). (C) The average density of the each layer and area of Wildtype (blue) and *M6a-/- M6b-/-* (red) brain at P7. The density of layer II/III in all area were normal and over all cell density was normal in the *M6a-/- M6b-/-*, except the density of the layer IV, V, VI in the visual cortex were significantly different (* $p<0.05$ by Student's t-test),

Figure 10. Abnormal callosal pathfinding in the *M6a-/- M6b-/-* mutant cortex. (A) The method for axon labeling. plasmid of GFP were injected to the embryo at E15.5 to label the layer II/III callosal neurons. (B-C) GFP expression in the wildtype (B) and in the *M6a-/- M6b-/-* mutant (C). the area of motor and somatosensory were labeled in both cases. (D-M) The sections with GFP staining. Matched coronal sections of wildtype (D) and in the *M6a-/- M6b-/-* mutant (E) are shown. Asterisks show the DNA injected side. The CC labeling at the midline are shown in (F) and (G), which are the magnified images of (D) and (E), respectively. The contralateral cortex of DNA injection in the wilftype (H) in the *M6a-/- M6b-/-* mutant (J) and ipsilateral cortex of the wilftype (I) in the *M6a-/- M6b-/-* mutant (K) are shown. The borders of Layer IV and V, (upper dotted lines) and Layer V and VI (lower dotted lines) were determined by Dapi staining. The striatum of (L) the wilftype (L) in the *M6a-/- M6b-/-* mutant (M) are shown. There were prominent axon bundles in the striatum of the *M6a-/- M6b-/-* mutant (arrowhead in M). Scale bars, 500μm (D, F, L), 250μm (H).

Figure 11. Single cell labeling for the wildtype mice. (A-E) Drowing of the projections based on the reconstited images of the single cell labeling. (A) shows overall projection in the wildtype at P7. Astarisks shows the positions of the cell bodies whose trajectories are picked up in (B-E). The dotted line shows the border of Layer Ⅳ and Ⅴ determined by Dapi staining. Scale bar, 2.0 mm.

Figure 12. Single cell labeling for the *M6a*-/- *M6b*-/- mice. (A-F) Drowing of the projections based on the reconstited images of the single cell labeling. (A) shows overall projection in the *M6a*-/-*M6b*-/- at P7. Astarisks shows the positions of the cell bodies whose trajectories are picked up in (B-F). The dotted line shows the border of Layer Ⅳ and Ⅴ determined by Dapi staining. Scale bar, 2.0 mm.

Figure 13. Impairment of the neurite outgrowth of the cortical neuron in mutant. (A-F) Cortical neurons prepared from wildtype (blue), *M6a*-/- (green), *M6b*-/- (yellow), and *M6a*-/- *M6b*-/- (red) embryos at E18.5 and cultured for three days. The axons were immunolabeled by anti-Tuj-1 antibody (tublin marker) and the average of axonal length and dendrite length elongated from one neuron were quantified. Total neurite length (axon and dendrites) (A) was significantly different in wildtype and *M6a*-/- *M6b*-/- ($*$ $p<0.05$ by multiple comparison of Tukey's test), as well as axonal length (B). There is no significant difference in dendrite length(C). Cortical neurons were sorted into BrdU-positive layer II/III neurons and BrdU-negative other layer neurons by the injection of BrdU at E15.5 (D-F). Total neurite length were significantly different in both types of neurons (D).

Figure 14. Rescue of impaired neurite outgrowth in the double mutant neurons by any of the M6 proteins. (A) Plasmids encoding EGFP-tagged M6a, M6b and DM20 were transfected into the layer II/III cortical neurons of the *M6a*-/- *M6b*-/- by in utero electroporation, and the neurons were cultured for three days. The axons were immunolabeled by anti-Tuj-1 antibody and the neurite length of GFP positive neurons were measured. (B) Effect of M6a over-expression on the neurite length of the wildtype neurons. Average neurite length of cortical neurons injected either GFP (blue) or M6a-ires-EGFP (green) to the wildtype were shown. There is no significant difference in the neurite length of GFP and M6a-GFP positive neurons,
(C) Rescue of the neurite length by the expression of M6 proteins in *M6a*-/- *M6b*-/- cortical neurons. Average neurite length of cortical neurons of the *M6a*-/- *M6b*-/- mice injected GFP (blue), M6a-ires-EGFP (green), M6b-ires-EGFP (yellow) and DM20-ires-EGFP (purple) are shown. The neurite length of M6a-ires-EGFP, M6b-ires-EGFP, and DM20-ires-EGFP injected neurons were significantly different compared to that of GFP injected neurons ($*$ $p<0.05$ by multiple comparison of Tukey's test), (D) Mapping the functional domain of M6a for the axonal outgrowth. Average neurite length of cortical neurons of the *M6a*-/- *M6b*-/- mice injected GFP (blue), M6a-ires-EGFP (green), and each deletion constructs (M6a Δ105-128, M6a Δ105-114 , M6a Δ115-128 , M6a Δ238-278) are shown. (E) The neurite length of M6a-ires-EGFP, M6a Δ238-278-ires-EGFP injected neurons were significantly different compared to that of GFP injected neurons ($*$ $p<0.05$ by multiple comparison of Tukey's test). (F) The amino acid aliments of near the second intercellular domain (IC2) of M6a(top), M6b (middle), DM20 (bottom). The amino acids that are common to M6a are colored with green. TM2; the second transmembrane domain, TM3; the third transmembrane domain.

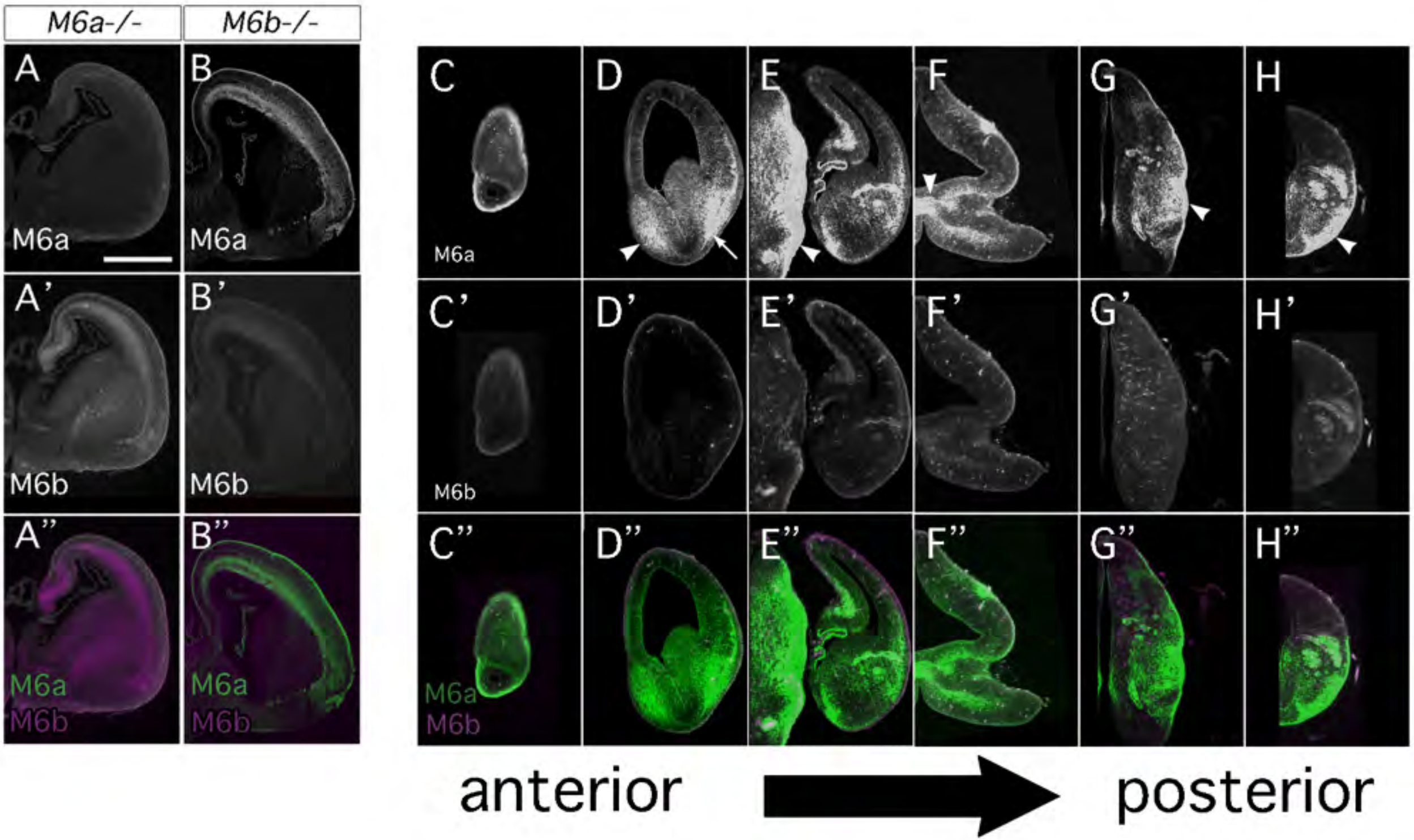
M6a-/-
M6b-/-
A
B
M6a
M6a
A'
B'
M6b
M6b
A''
B''
M6a
M6b
M6a
M6b
C
D
E
F
G
H
M6a
C'
D'
E'
F'
G'
H'
M6b
C''
D''
E''
F''
G''
H''
M6a
M6b
anterior
posterior

Figure 1.

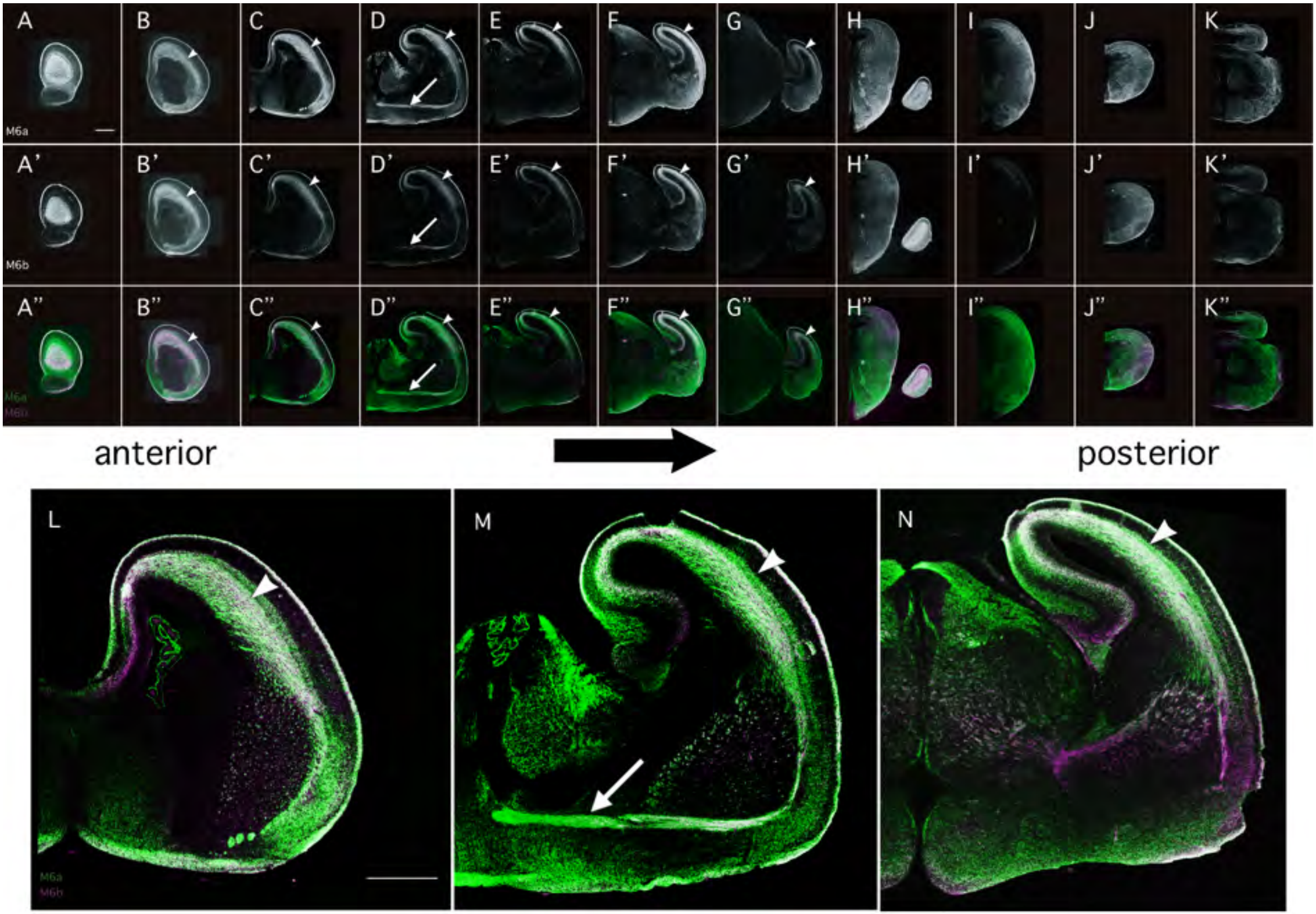
A
B
C
D
E
F
G
H
I
J
K
M6a
A'
B'
C'
D'
E'
F'
G'
H'
I'
J'
K'
M6b
A''
B''
C''
D''
E''
F''
G''
H''
I''
J''
K''
M6a
M6b
anterior
posterior
L
M
N
M6a
M6b

Figure 2.

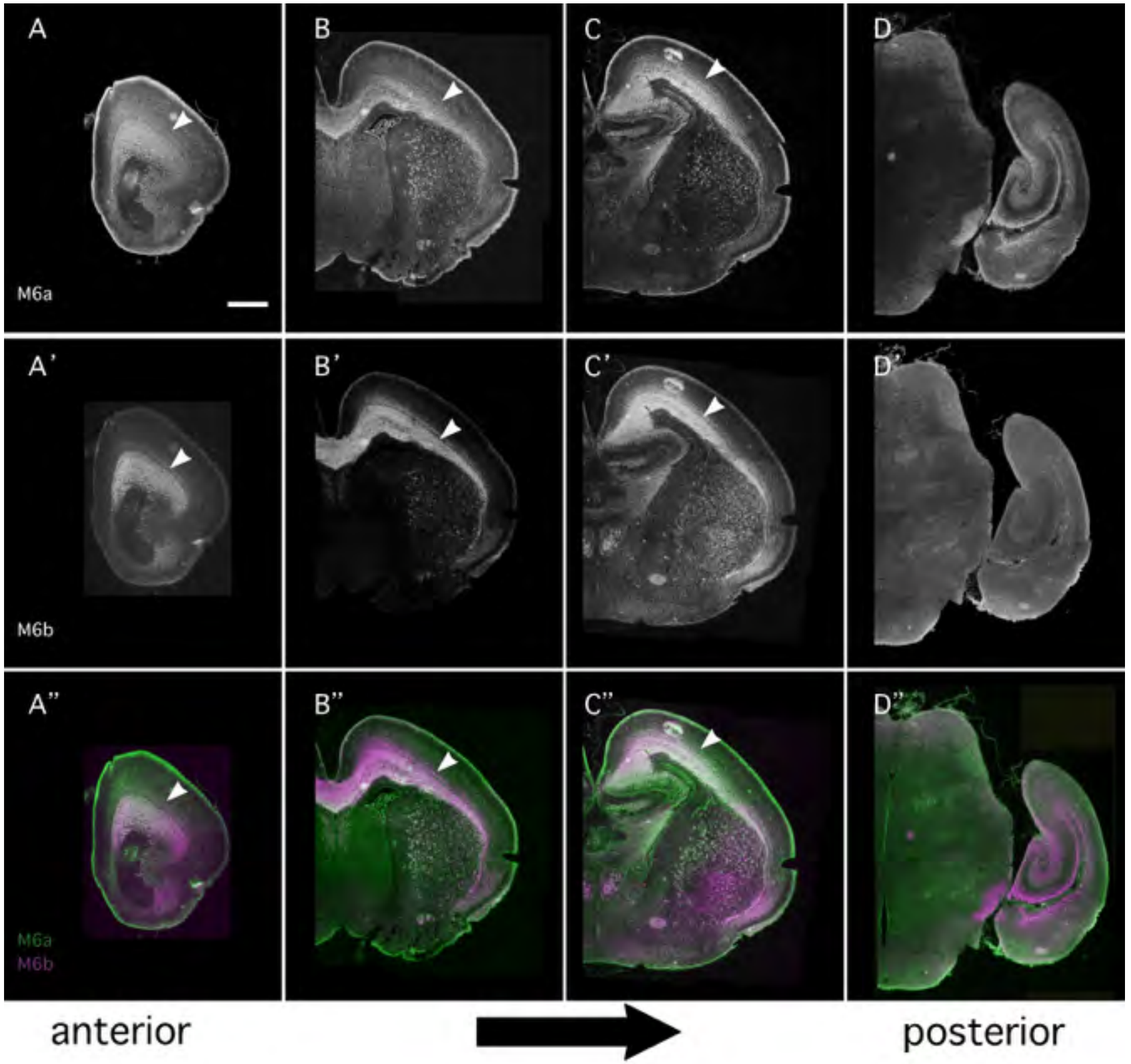

Figure 3.

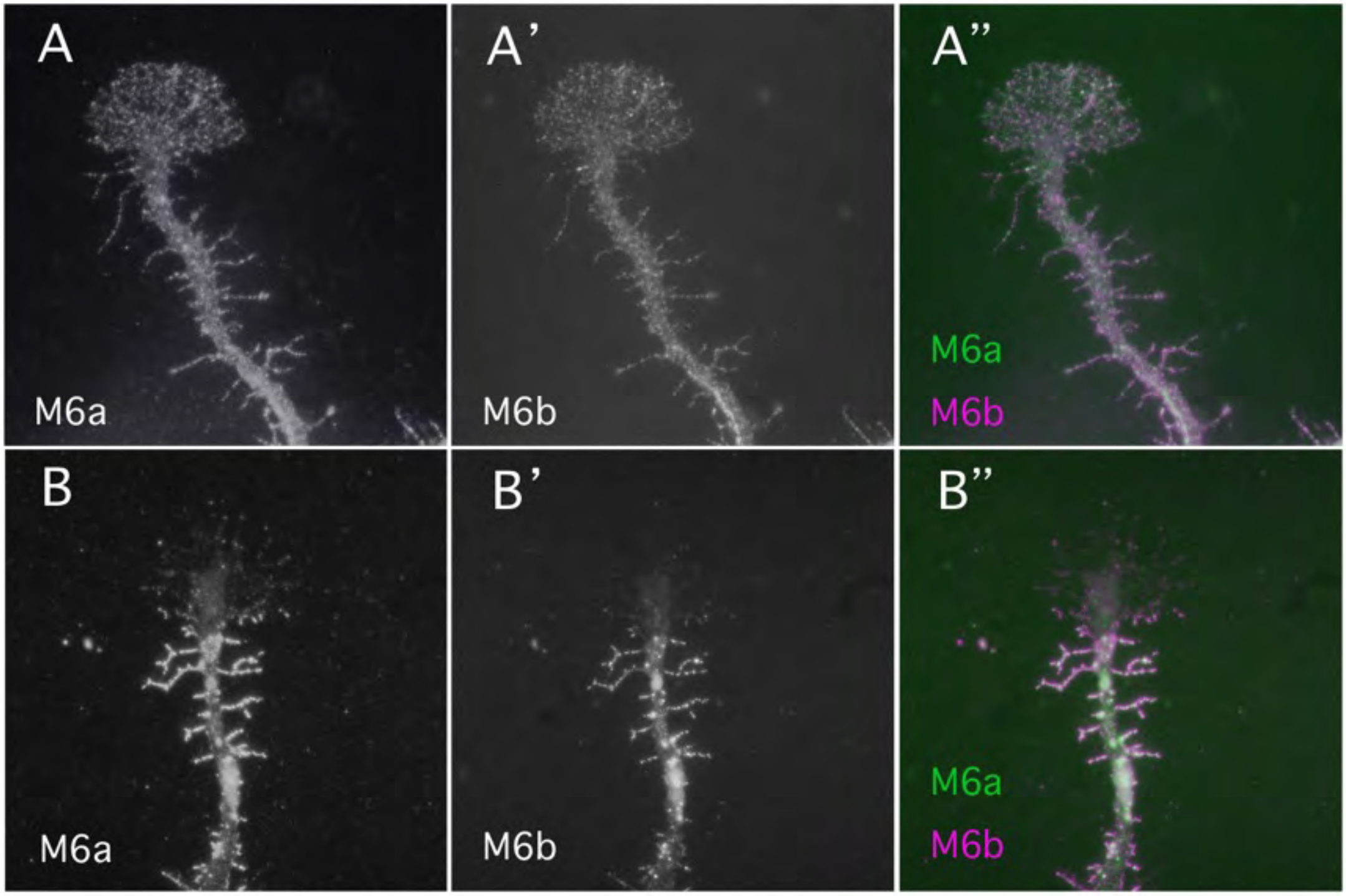

Figure 4.

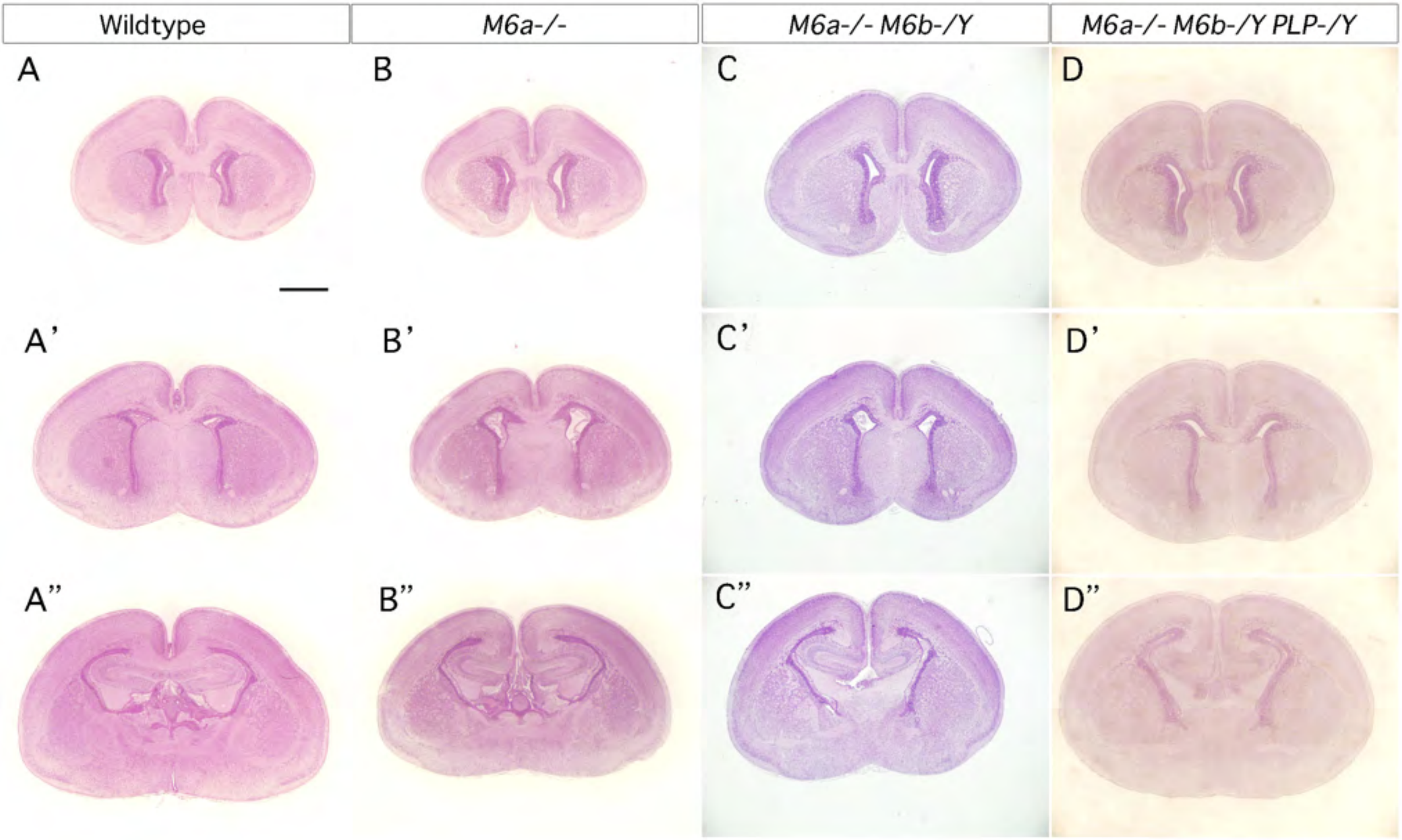

Figure 5.

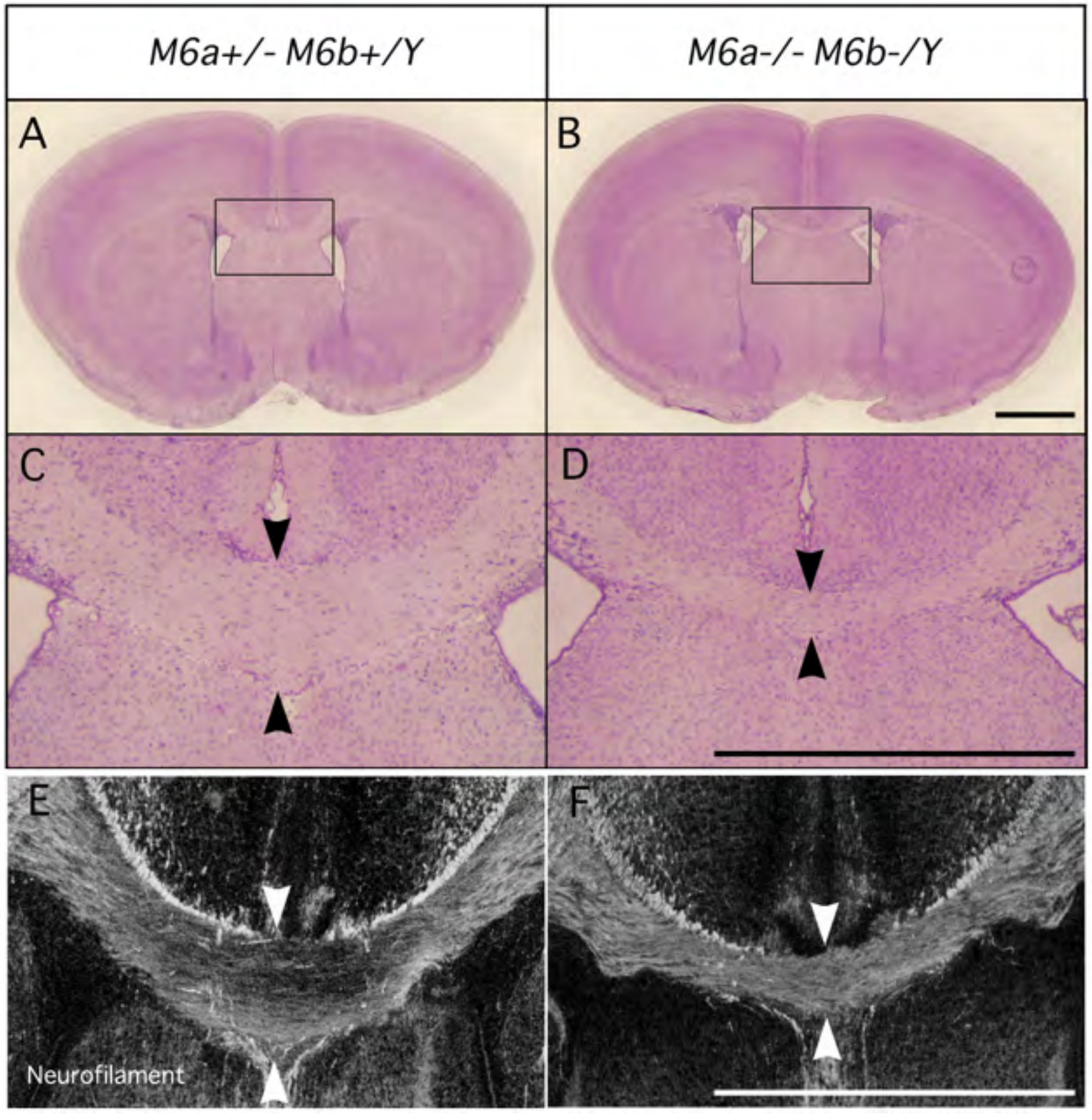

Figure 6.

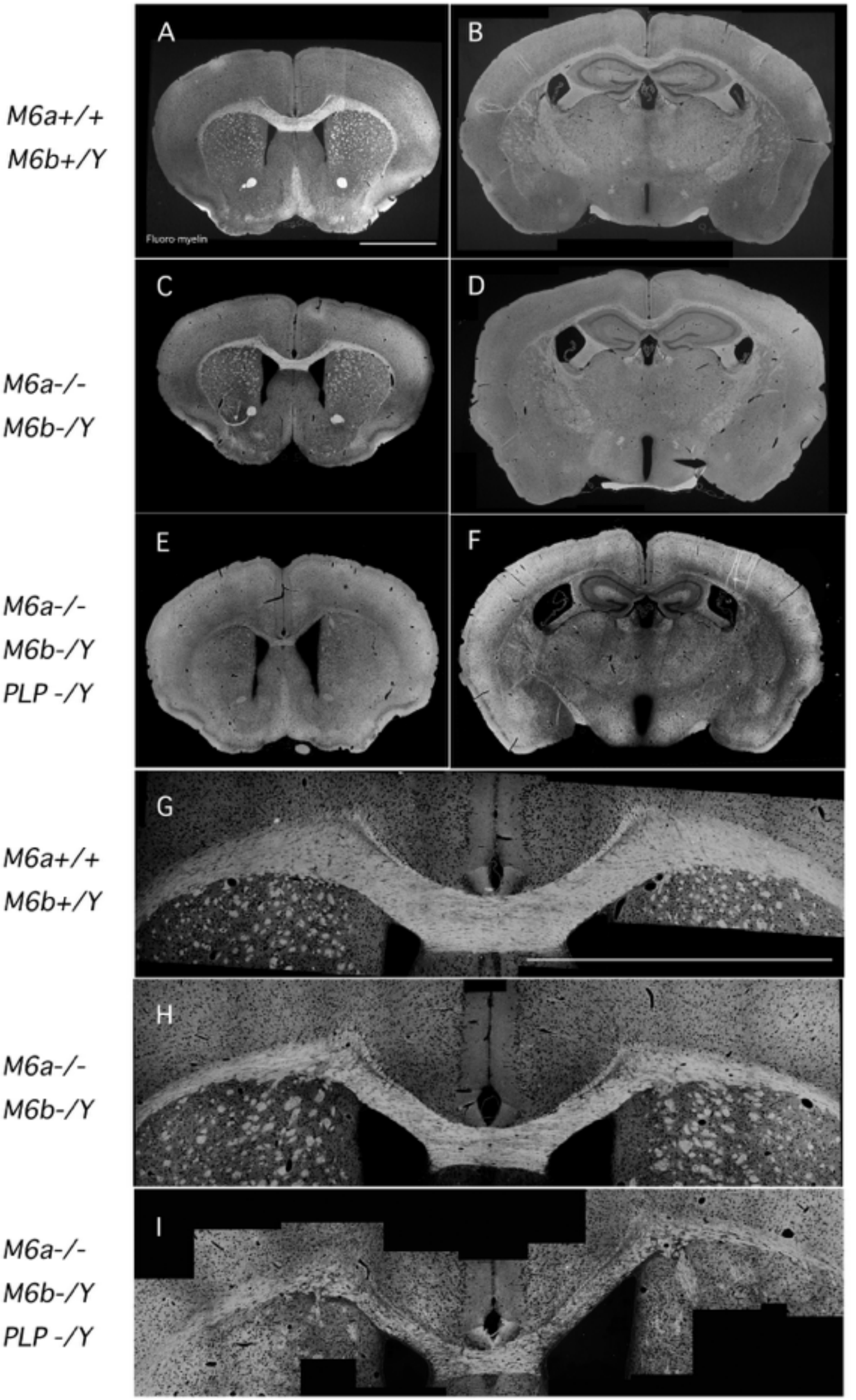
M6a+/+
M6b+/Y
A
Fluoro-myelin
B
M6a-/-
M6b-/Y
C
D
M6a-/-
M6b-/Y
PLP -/Y
E
F
M6a+/+
M6b+/Y
G
M6a-/-
M6b-/Y
H
M6a-/-
M6b-/Y
PLP -/Y
I

Figure 7.

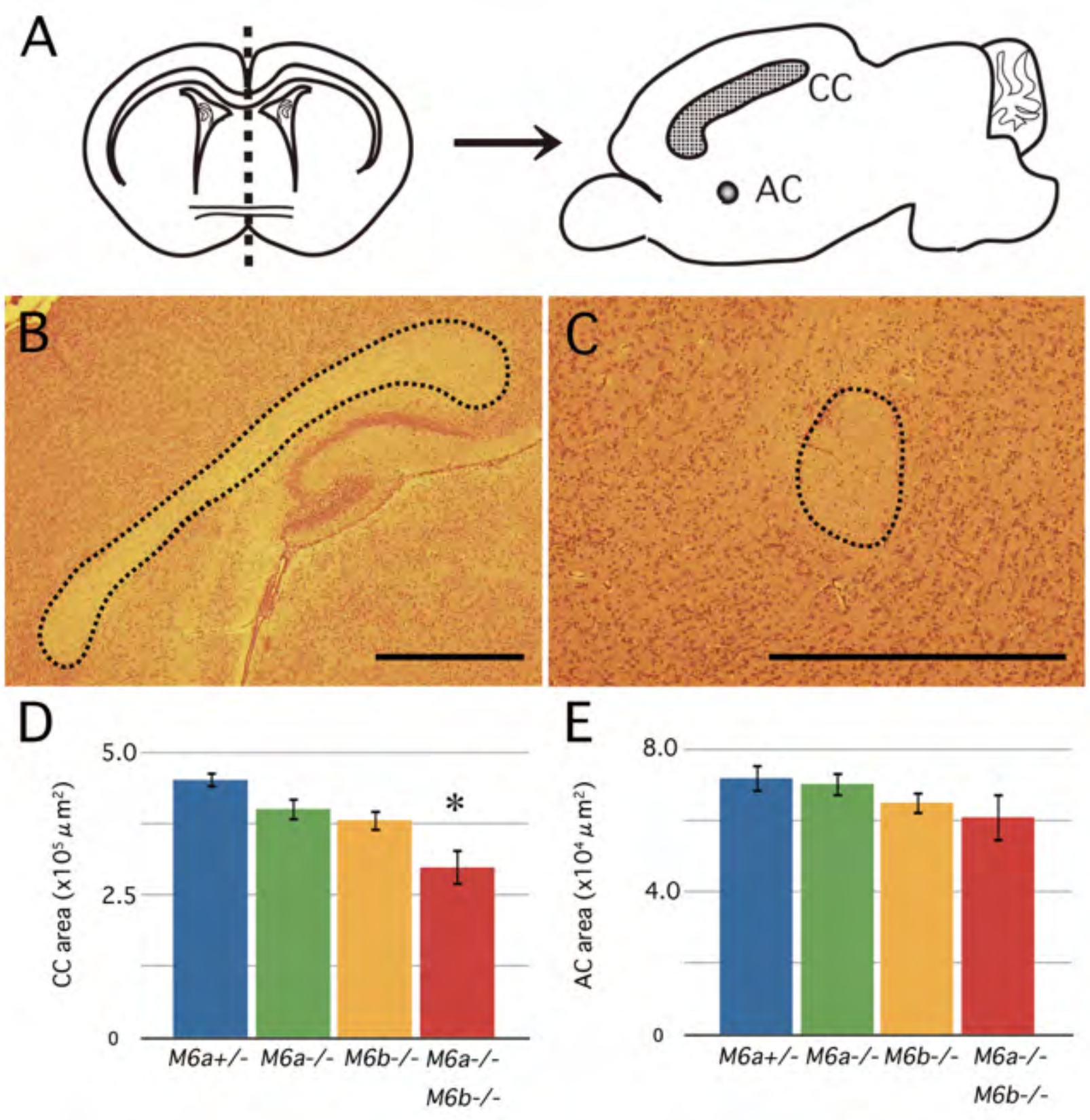
A
CC
AC
B
C
D
5.0
2.5
0
CC area (x10⁵ μm²)
*
M6a+/-
M6a-/-
M6b-/-
M6a-/- M6b-/-
E
8.0
4.0
0
AC area (x10⁴ μm²)
M6a+/-
M6a-/-
M6b-/-
M6a-/- M6b-/-

Figure 8.

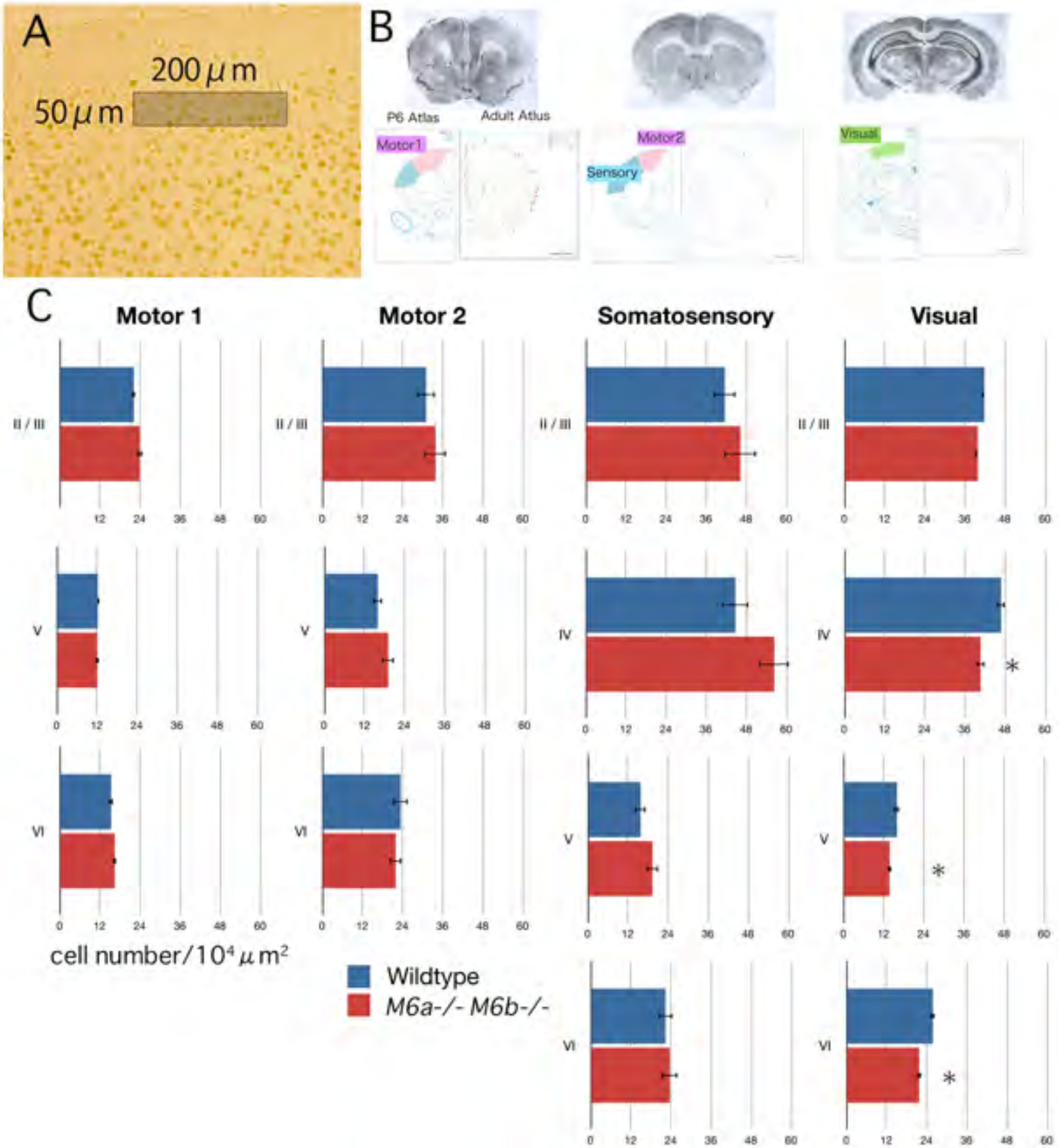
A
200 μm
50 μm
B
P6 Atlas
Adult Atlus
Motor1
Sensory
Motor2
Visual
C
Motor 1
Motor 2
Somatosensory
Visual
II / III
IV
V
VI
0 12 24 36 48 60
*
cell number/10⁴ μm²
Wildtype
M6a-/- M6b-/-

Figure 9.

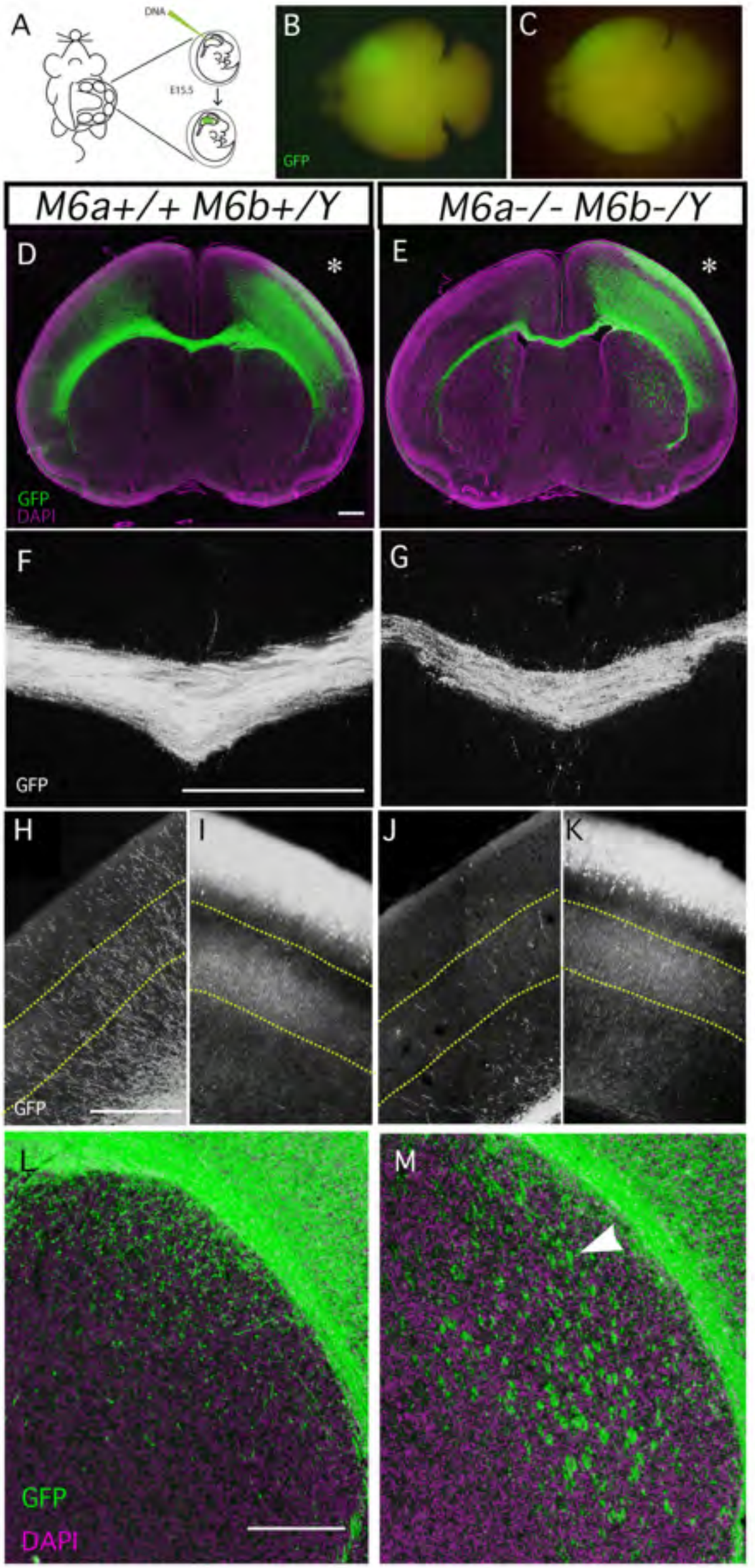
A
DNA
E15.5
B
GFP
C
M6a+/+ M6b+/Y
M6a-/- M6b-/Y
D
*
GFP
DAPI
E
*
F
GFP
G
H
I
J
K
GFP
L
GFP
DAPI
M

Figure 10.

Widltype

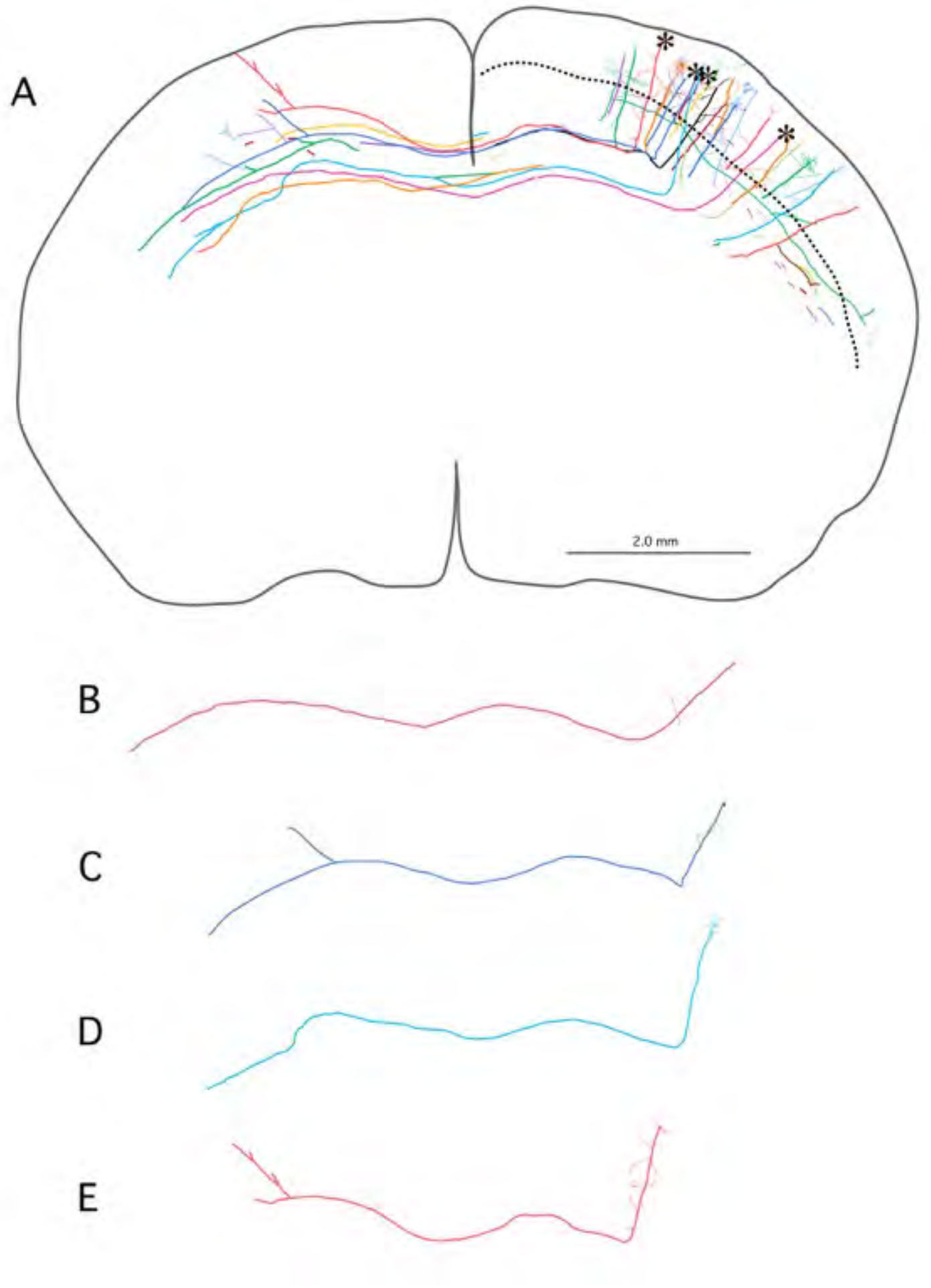

Figure 11.

M6a-/- M6b-/Y

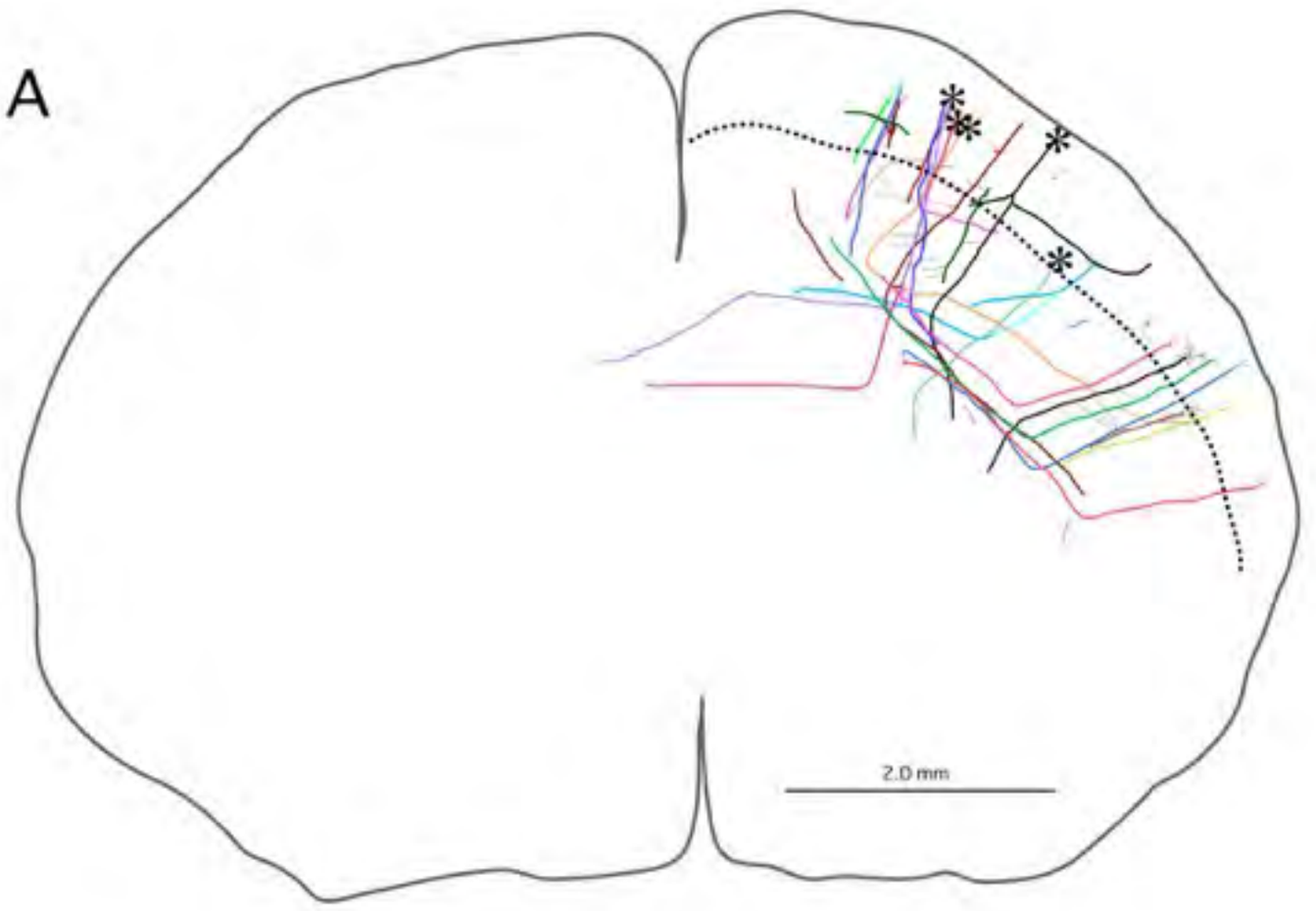

Figure 12.

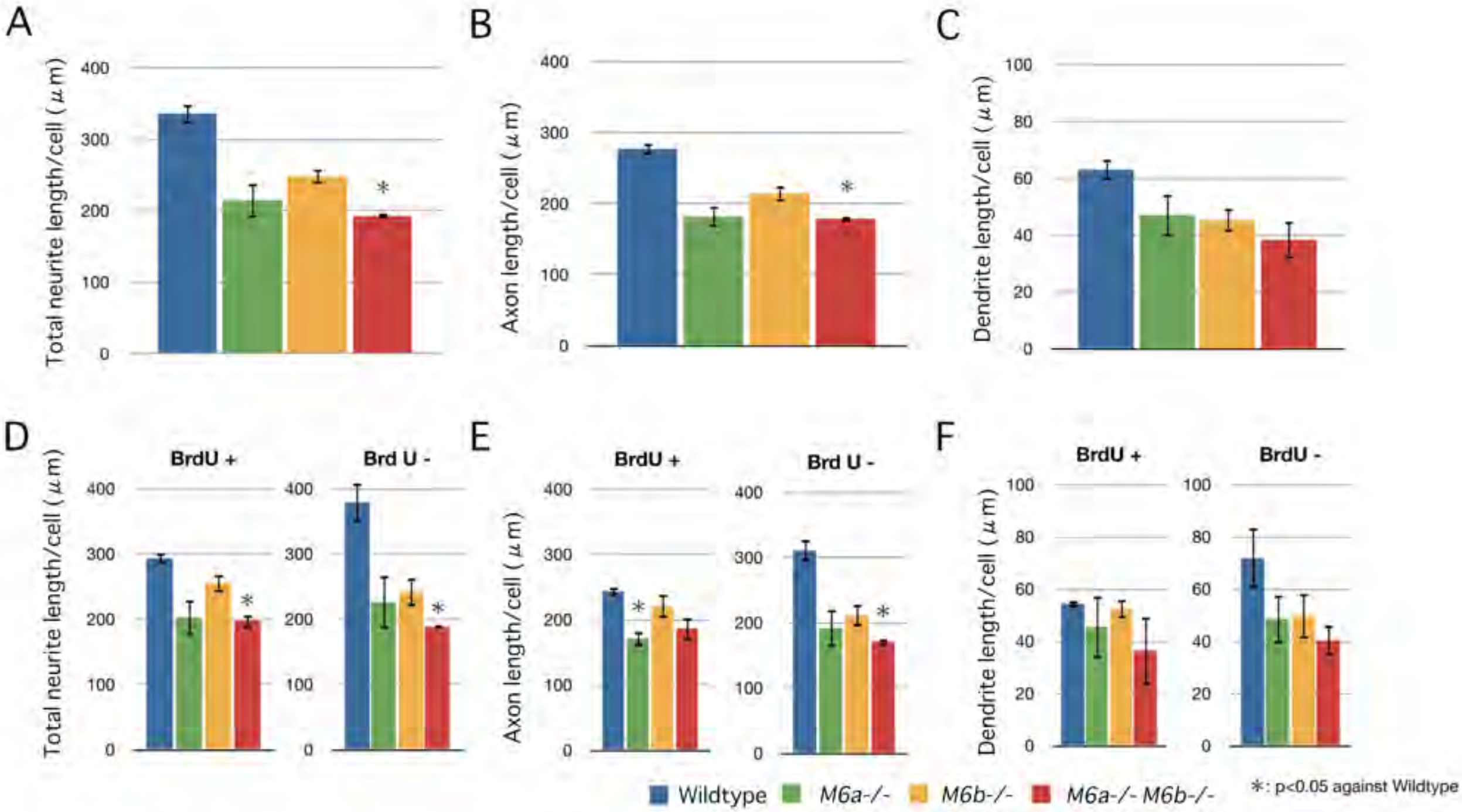
A
B
C
Total neurite length/cell (μm)
Axon length/cell (μm)
Dendrite length/cell (μm)
400
300
200
100
0
100
80
60
40
20
*
D
E
F
BrdU +
Brd U -
BrdU -
Wildtype
M6a-/-
M6b-/-
M6a-/- M6b-/-
*: p<0.05 against Wildtype

Figure 13.

A

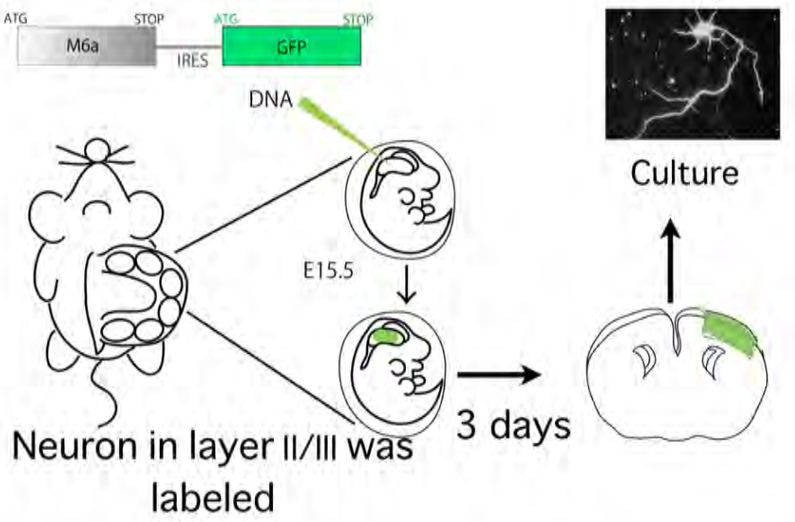

B

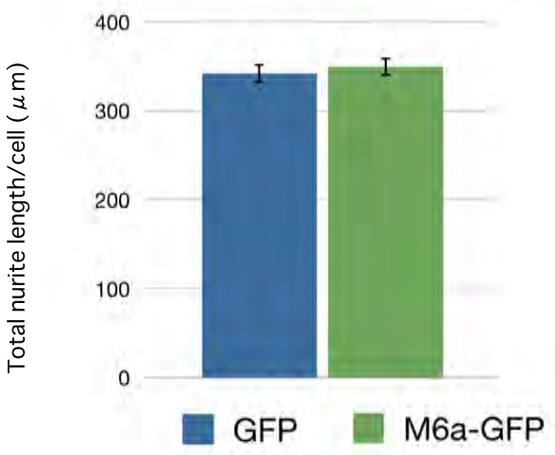

C

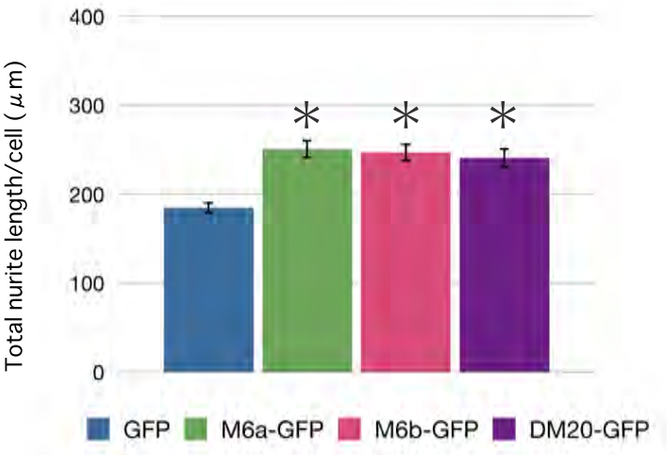

D

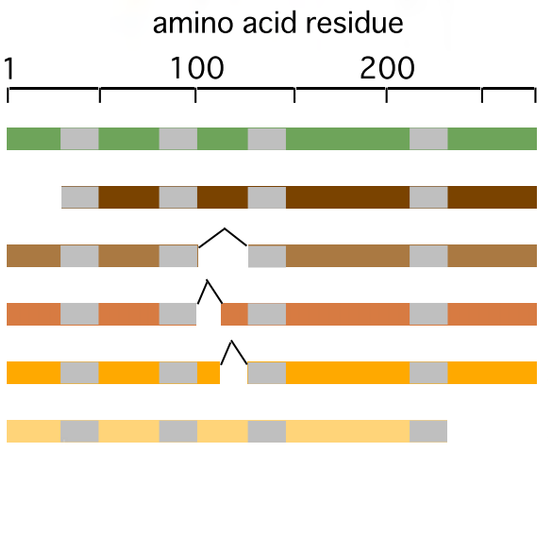

E

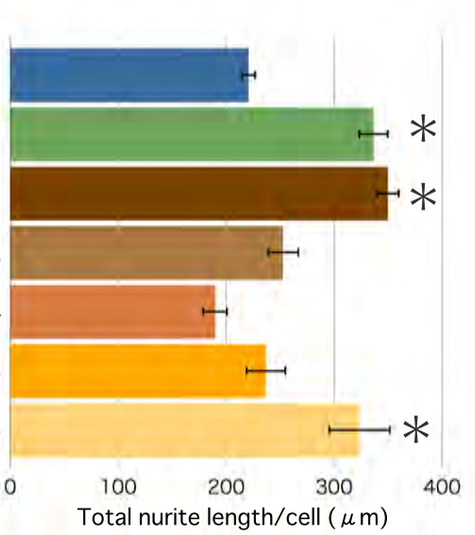

F

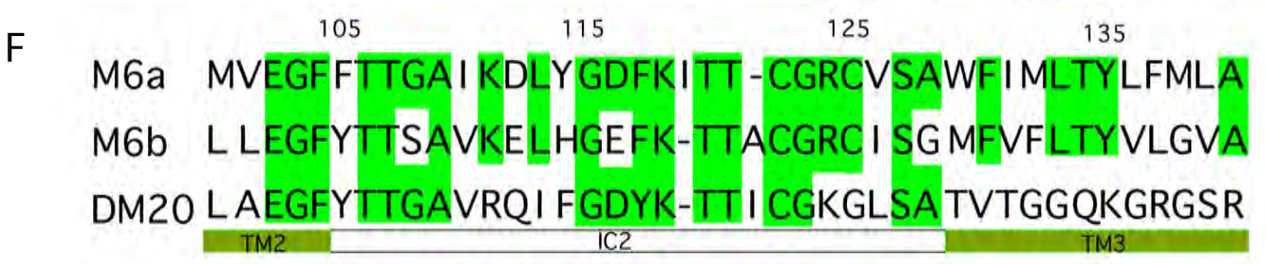

Figure 14.